CHARACTERIZING AIRFLOW PATHS IN GRAIN BULKS

BY

CHARLES CHIOMA NWAIZU

A Thesis submitted to the Faculty of Graduate Studies of

The University of Manitoba

in partial fulfillment of the requirement for the degree of

MASTER OF SCIENCE

Department of Biosystems Engineering

University of Manitoba

Winnipeg, Manitoba

ABSTRACT

Modeling of airflow resistance in grain bulk requires knowledge of the tortuosity and velocity of the air flow through the grain bulk. In this study, experiments were carried out to determine these characteristics of airflow paths by analyzing digital images of smoke-visualized airflow paths inside a grain bulk obtained with a high speed camera. Colored smoke with approximately the same density as air was introduced into the test box for the visualization of the airflow through the grain bulk. Soybeans with a moisture content of 8.82% on wet basis were used in this study. The high quality videos obtained by recoding the fast movement of the smoke through the grain bulk was first separated into frames using a commercial software, VirtualDub (CRIM, Montreal, Québec, Canada), and the 512× 384 pixel RGB image files (frames) extracted from the recorded videos and read into ImageJ an image processing Java-based software developed by the United State National institute of Health, to track the movement of the smoke in the images, frame by frame to determine lengths, tortuosities of the different flow paths, as well as their velocities.

ACKNOWLEDGEMENTS

I owe a deep and sincere gratitude to my Advisor, Dr. Qiang (Chong) Zhang for his support and guidance throughout my M.sc. programme. I am always amazed by his inestimable depth of knowledge and experience. His contribution in improving my writing skills are highly cherished and appreciated. I would also like to thank members of my advisory committee; Dr. Ramanathan Sri Ranjan and Dr. Oluwole Akinremi for their contribution and valuable suggestions during committee meetings.

I wish to appreciate the Natural Science and Engineering Research Council of Canada (NSERC) for their financial support to this project. Also, I sincerely thank the technical, administrative and academic staffs in the department of Biosystems Engineering for all their assistance and support during the course of my programme.

I would like to use this medium to specially thank my father for making me to believe that I can do all things if only I believe in myself and God. And it is my mother that made me to understand that there is always a gain in being diligent at your work. I am indebted to my sisters, they are all my beginning and they still stick to me to this very moment – I love you guys!

To my friends Wale, Idris, Nonso , Bayo, Yvonne, Princess Ibeneme, Sylvia, Rong, Pablo, Chaoli, Amy, Ivy, Johnson and all the members of the Redeemed Christian Church of God, thanks for being there and may we always remember that dreams create the future and our greater times are yet to come.

Lastly, my utmost gratitude goes to the cause that has no cause, the unmovable mover, the King of kings – the Almighty God, without whom there wouldn't have been any progress or any life accomplishment!

DEDICATION

This thesis is dedicated to my father: Mr. Christopher Nwaizu (Onyemalusa) for his unflinching love for education and the roles he played in my life as a young boy, teaching me arithmetic and elementary sciences which later leads to my love for Science and Engineering.

TABLE OF CONTENTS

5. CONCLUSION AND RECOMMENDATIONS

LIST OF TABLES

LIST OF FIGURES

1. INTRODUCTION

The world production of grain amounts to approximately 1.8 million tonnes per year. Canada produced on average 60.1million tonnes of these grains each year over the period from 2008 to 2011(IGC, 2012). Preservation of grains until it is ready for consumption by human and domesticated animals has been a major preoccupation of mankind since the inception of agriculture. Over the years, aeration and drying practices have been the common methods used for grains preservation. However, failures of some of these drying and aeration methods have triggered studies of airflow distribution in the grain bulks (Gayathri et al., 2007).The knowledge of resistance to airflow through grain bulks is fundamental in efficient design of grain drying and aeration systems. (Shedd, 1951; Crozza et al., 1995; Pagano et al., 2000; Lukaszuk et al., 2008; Shahbai, 2011). Basically, the airflow resistance has always been empirically obtained by the measurement of pressure drop along a bed of material being tested at different flow rates. Empirical curves for various grains that have been established for pressure drop along the bed of the grains by Shedd (1951) and Hukills and Ives (1955) have been adopted in the standards of the American Society of Agricultural and Biological Engineers (ASABE R2011.D272.3, 2011).

Navarro and Noyes (2002) showed that the values of the airflow resistance obtained from these empirical curves were based on the assumption that resistance to airflow is constant in the volume of the grain bulks and independent of its pore structure. This assumption contradicts the results reported by other researchers, who showed that variables like grain kernel size, shape, bed height, porosity, airflow velocity, airflow direction, moisture content, filling methods, pore structures all have a significant effect on airflow resistance through grain bulks (Calderwood, 1973; Stephen and Foster, 1976; Kumar and Muir, 1986; Hood and Thorpes, 1992; Neethirajan et al, 2006; Lukaszk et al., 2008; Shahbai, 2011). Wu et al. (2006) developed an airflow resistance model for porous media that not only was expressed as a function of porosity, particle size and shape, but also assumed that the capillaries in the porous

medium were tortuous, unlike the fundamental Ergun's airflow resistance model, in which the tortuous nature of airflow in the porous media was not considered. The tortuous flow of air in the porous media is often quantified by a parameter known as tortuosity (τ). This concept of tortuosity was first introduced by Kozeny (1927) and was later mathematically explained by Carman (1937). Generally, tortuosity (τ) is defined as the ratio (or the square of the ratio) of the effective length (L_{eff}) of the flow path through the porous media to the apparent length (L_{app}).

$$\tau = {}^{L_{eff}}\!/_{L_{app}} \tag{1}$$

where:

τ =tortuosity

L_{eff} = effective length (m)

L_{app} = apparent length or flow path (m)

This equation shows that a straight channel has a tortuosity of one, while the tortuosity of a channel going through a grain bulk has a tortuosity value greater than one. Theoretical models have been developed to predict the value of tortuosity in grain bulks (Gayathri et al., 2007). Most of these models used the shortest length or the average of various flow lengths as the effective path length through the grain bulk (Maciej et al., 2008; Sobieski et al., 2012). Also, there have been many experimental methods that led to indirect estimation of tortuosity. Measuring a quantity termed the formation factor obtained from the resistivity measurement of a given fluid in a porous medium of a known porosity, many researchers have been able to indirectly estimate the values of tortuosity for different porous media (Wyllie and Spangler, 1952; Winsauer et al., 1952; Cornell and Katz, 1953; Faris et al., 1954; Pirson, 1983; Garrouch et al., 2001; Attia, 2005). Garrouch et al. (2001) estimated the tortuosity of a variety of sandstone rock samples to be in the range of 2 to 4. Attia (2005) in his study of rocks with porosity between 0.2 and 0.3 obtained the values of tortuosity between 1.3 and 2. Another common method for the determination of tortuosity is through the results from diffusion measurements, by relating

the diffusion coefficient measurement of a fluid in the porous media to the tortuosity (Faris et al., 1954; Brakel and Heertjes, 1974; Dogu and Smith, 1975; Barrande et al., 2007). Based on this principle, Choudhary and Horwath (1997) determined the tortuosity of various siliceous packed in a column to be between 1 and 1.3 for a porosity of 0.5. In a study of diffusion with different sizes (ranges from 30 - 40μm) of fixed bed glass beads, Barrande et al. (2007) estimated the tortuosity values to be between 1.3 and 2.5.

Also, pressure drop measurement across bulk particles, has been used by Comiti and Renaud (1989) for indirect estimation of tortuosity. Techniques like the mercury intrusion porosimetry and ultrasonic reflectivity have been suggested by Webb (2001) and Fellah et al. (2003) respectively for indirect determination of tortuosity. The indirect determination of tortuosity sometimes may results in unrealistic values of more than one thousand (Papadokostaki et al., 1998) or below one (Foster and Parrott, 1990). Direct measurement of flow path length in porous media is possible when image analysis is used. However, little information is available in the literature on the direct determination of tortuosity from actual flow paths in grain bulks.

In this research an image visualization technique was employed to achieve the following objectives:

1. to directly measure tortuosity and airflow paths in grain bulks and
2. to study the effect of the airflow rates and fill density on tortuosity and flow velocity in the grain bulk.

2. REVIEW OF LITERATURE

2.1. Physical properties of grain bulks

2.1.1. Geometry

The geometry of grain kernels affects the air flow through the grain bulks (Cenkowski and Zhang, 1995). Measuring the size of grains is very important in drying and aeration process to determine airflow rate (Muir et al., 2005). The shape of grain kernels is another important geometric property of a grain bulk, which is very important in the studies of airflow through grain bulks (Yuichi et al., 2005). Lukaszuk et al. (2008) demonstrated that the grain kernel size and shaped influenced the airflow resistance. He stated that at an air velocity of 0.3 m s^{-1}, the air flow resistance was between 32±0 4Pa for pea and 135±1.7 Pa for rapeseed. Neethirajan et al. (2006) stated that the airflow resistances in the vertical and horizontal direction of wheat, barley and flax seeds are different. They also stated that the airflow resistance in spherical seeds such as pea and mustard bulks was lower compared to wheat, barley, and flax seed.

2.1.2. Density

The density of a grain bulk is a very important physical property that affects airflow resistance. It is expressed as the ratio of the total mass of the grain to its volume.

Fashina (2007) explained the four different ways to describe the mass- volume ratio (density) of grain bulks as follows:

Bulk density: It is the ratio of the mass of the bulk that filled a given container to the volume of the container.

Apparent particle Density: It is the ratio of the mass of a sample particle of a grain bulks to the solid volume, occupied by the particle, with the open and closed pores considered.

True Particle Density: It is the ratio of the mass of a sample particle of a grain bulks to the volume occupied by the particle, without considering the open pores.

All the measured densities of the grain particle and bulk are very important parameters that affect milling and breakage susceptibility (Chang, 1988). They are also very important in designing near- ambient drying and aeration systems, because they affect resistance to airflow of stored grain bulks (Navarro and Noyes, 2002). Although, most times, the true particle density has been used interchangeable with the apparent particle density, Fashina (2007) not only cited differences in their measurements, but also stated that the true particle density was more appropriate for use in ventilation and drying operations, while the apparent density was appropriate for use in airflow flow problems around grain bulks. Also, bulk density influences the market value and grade of grain bulks (Jayas and White, 2001).

There are several factors that affect the bulk density of grain, such as the moisture content (Shahbazi et al., 2011). Bulk density decreases slightly with increase in moisture content. Dutta, (1988) obtained the value of bulk density of gram grain to vary from 780 to 708kg m^{-3} as the moisture content varied from 9.68 to 31.0%. Stuart (1980) showed that for wheat the bulk density linearly increased slightly as the moisture content increases from 3 to 8% and then decreased continuously as the moisture content increased. And for corn grains, the bulk density decreased continuously with increase in the moisture content. Karababa (2006) concluded that the bulk density of popcorn kernels decreased linearly from 0.771 to 0.703 as the moisture content increased from 8.95 to 17.12%. Same conclusion was obtained for the particle density of grain bulk, which tends to decrease as the moisture content increases (Karababa, 2006).

Other factors, such as size of the grain kernels and insect infestation have, also shown considerable effect on the bulk density of the grain bulks. Adams (1972) reported that insect attacks on wheat, corn and Sorghum reduced the bulk density, and the reduction in the bulk density was directly proportional to the dry weight consumed by the insect. The methods of filling grains into bins affect the bulk density of grain bulk. Lukaszuk et al. (2008) used axial

gravitational filling methods with grain falling from heights of 0, 0.95 and 1.9m over the bin floor produced bulks of densities in of 773, 790 and 810kg m^{-3} respectively. There are many standard methods for determination of bulk density for bulk solids materials, including bulk grains (ASAE D241.4; ASABE Standard, 2008), aggregates (ASTM C29; ASTM, 2007b), particles (ASTM F1877; ASTM, 2005). Those methods typically involve a measurement apparatus in which a given container with a known volume is filled with the materials and the bulk density is then estimated as the mass of the material that filled the container divided by the volume of the container. An example was the method used by Clementon et al., (2010) for measuring the bulk density of grains and oil seeds, which involves falling of grain due to gravity from a funnel into a container and the mass of the grain in the container divided by the volume of the container as taken as the bulk density.

This method involves filling a cup through a hopper and then the weight of the materials that filled the cup and the volume of the cup are obtained for estimation of the bulk density. Studies by Shinohara et al. (1972) and Standish (1985) showed that variation in the falling height of the material through the hopper into the cup influenced the bulk density measurement.

There are two common methods for the measurement of particle density, the liquid-displacement method and the gas displacement method (Fang et al., 2000), and both methods have successfully been used in determination of particle density of grain bulks. However, the surface tension characteristics of most liquids, like water or mercury, possess a problem in adequately using liquid for the determination of void space volumes for most grain and seed kernels (Chang, 1988).

The gas displacement method gives a rapid and accurate result in measuring the volume of grain kernels, and the use of inert gases such as helium eliminates any reaction between the gas and the grain particles during measurement (Robert et al., 1972). Many

researchers have used gas pycnometers to measure the volume of grain and seed kernels for estimating the particle density (Marinder 1996; Tanari, 2004).

Fashina (2007) employed a pycnometer to measure the true particle density of agricultural materials (wheat, corn, rice, brown, popcorn, chickpea, lima bean, black eyed beans, and pinto beans) and he reported that the particle density obtained from the pycnometer was not the true particle density because some of the pores in the grain kernel were included in the determination of the kernel volume. A similar observation was made by McMasters (1962).

2.1.3. Porosity

In the modeling of grain bulk processing operations like drying, aeration, heat transfer and other similar operations, information about the volume of voids present in the bulk is important (Navarro and Noyes, 2002). The void volume is commonly measured as porosity, which is defined as the ratio of the void volume to the total volume of the bulk. The porosity is related to the particle and the bulk density as follows (Mohsenin, 1980).

$$\varepsilon_t = 100\left(1 - \frac{\rho_b}{\rho_{pt}}\right) \tag{2.1}$$

where:

ε_t= total porosity (%)

ρ_b= bulk density ($kg\ m^{-3}$)

ρ_{pt}=particle density ($kg\ m^{-3}$)

The porosity obtained from the equation (2.1) is refer to as the total porosity (Fasina, 2007), while the particle porosity and the bulk porosity can be calculated from the equation (2.2) and (2.3) respectively.

$$\varepsilon_b = 100\left(1 - \frac{\rho_b}{\rho_{pt}}\right) \tag{2.2}$$

$$\varepsilon_s = \varepsilon_t - \varepsilon_b \quad (2.3)$$

where:

ε_b= bulk porosity (%)

ρ_b= bulk density ($kg\ m^{-3}$)

ρ_{pt}=particle density ($kg\ m^{-3}$)

It was stated by Fasina (2007) that the total porosity is always expected to be greater than the bulk porosity for a given grain bulk.

Generally the porosity of a grain bulk is affected by several factors, similar to the bulk density and particle density. Nimkar and Chatttopadhyay (2002) revealed that the porosity of grain bulk increased with increased moisture content. Specifically, when the moisture content changed from 8.36 to 16.65%, the porosity increased from 42.15 to 43.64%. Similar trends in relationship between porosity and moisture content were reported by Karababa (2006). Thompson and Isaac (1969) observed that the porosity of shelled corn was affected not only by moisture content, but also by the method of harvest, method of drying, and variety. For shelled corn that was dried from 25.7% to 14.7% and then to 9% moisture content, its porosity decreased from 44.28% to 40.45% and then 38.64% respectively. Corn harvested with combine had porosity of 41.06%, and after the removal of the broken kernels, the porosity was to 40.27%. This showed that removing the broken kernel resulting from harvesting caused reduction in the porosity because the presence of the broken kernels increased the void space.

It was also revealed in their conclusion that when an artificial drying method was used in drying the shelled corn from a moisture content of 30.8 to 8.5% the resulted porosity was found to be 44.49% which was higher than the porosity of 38.64% of a similar sample dried with ambient air. The determination of porosity for grain bulks can be achieved by several methods, which aim to measure the void volume and the volume of the grain bulk (Fasina, 2007). Rajabipour et al. (2001) measured the porosity by pouring a known quantity of water into

container containing walnut grains. Shahbazi (2011) used toluene instead of water to determine the porosity of chicken pea seeds. The use of gas as the displacing medium for determination of porosity (gas pycnometer) has become popular among researchers; because liquids are not adequately suited for the determination of pore space of most grains and seeds (Tamari, 2004). Other techniques, such as the X-ray CT, have been used in the estimation of porosity (Taud et al., 2005).

2.1.4. Pore Structure

There have been many significant studies about the characterization of pore structure in geological or geotechnical porous media. However, apart from the investigation of the geometry and the interior interconnectivity in grain bulks using X–ray CT images by (Neethirajan et al., 2008), the study of pore structure has been limited in grain bulks, despite the importance in understanding the interior structure of grain bulk. Smith and Jayas (2004) cited that information about the interconnectivity of airflow paths is needed in design of forced ventilation and in modeling heat transfer inside grain bulks. And the pore size distribution is very important in developing link between the grain bulks microstructure and its macro drying behavior (Nielsen, 1998).

Also, information about the pore space network in grain bulks will enhance predictive model for insect movement in the grain bulks (Jian et al., 2005) and aid in understanding sound transmission through grain bulks and consequently, facilitate design of acoustic systems for detecting insect infestation in the stored grain (Hickling,1997). Neethirajan et al (2008) concluded in their study that linking the pore geometry to the measurement of conductivity parameters will increase the accuracy of models used in predicting conductivity in grain bulks. Hood and Thorpes (1992) stated the importance of understanding the interior structure of grain bulks succinctly: “It will be possible to completely calculate the velocity field of fluid flow within a

bulk of grains provided that the geometry of the inter-phase boundaries be quantified and specified".

The pore structure in porous media can be defined in terms of the sizes, shapes or paths of the relative narrow spaces (also called void) enclosed between particles in the porous media, which are microscopically connected to form a complicated network of channels (Bear, 2007). Although, there have been difficulties to perfectly describe the irregularity of pore geometry in a porous medium, many researchers have used different approximate techniques in order to model the pore structure in porous media. A simple model known as the straight tube geometry model, in which bundles of cylindrical capillary tubes of different diameters and equal lengths are used to approximate the pore structure (Bear, 2007) has become acceptable. However, this simple model does not adequately describe the heterogeneity of porous media and the interconnectivity of pore spaces. Other models, like the pore-network model have been developed using symmetric regular 2 or 3-dimensional network to represent the pore structure of a porous medium. Kammath et al. (1998) used the pore network model to explain the pore structure of rocks. Jian et al. (2005) applied the pore network model to grain bulk to predict the distribution of temperature, moisture and pressure during grain drying.

Determination of the pore structure characteristics such as pore size, pore shape, pore surface area, pore volume and distribution is important in understanding the internal structure of a porous medium. Mercury intrusion porosimetry and sorption isotherm are well established techniques for measuring pore size distribution (Bear, 2007). Although mercury intrusion porosimetry uses a toxic substance and high pressures, it is more popular compared to sorption isotherm, because it is versatile, that is, it can be used with almost any type of porous media(Dullian, 1991).

In mercury intrusion porosimetry, mercury is pressurized to enter the pores of the porous medium and the diameter of the pore and its volume can then be measured by

measuring the intrusion pressure and the volume of the intrusion liquid respectively (Sidney, 2000). Mercury intrusion porosimetry has been used to study different porous materials such as active carbons, adsorbent, various rocks, ceramics, plastic, Textile, wood and so on. (Dullian, 1991). However, the pore size distribution obtained from this method is not accurate due to geometric and other uncertainties (Bear, 2007). In order to improve the accuracy of mercury intrusion porosimetry, Dullian (1991) explained how the method could be combined with the optical method in measuring pore size distribution in clay soil.

The sorption isotherm is based on the principle of adsorption or desorption of gas or liquid in pores of the porous medium. It is mostly used for the measurement of small size pores, and gives accurate surface area of the pores (Florence et al., 2008). Water and nitrogen gas are most widely used for pore structure measurements (Florence et al., 2008). The thin sectioning method has been used to study soil structures (Nimmo et al., 2004). Measurements of pore size distribution obtained from the thin section method compared favorably with the results obtained from other methods (Nimmo et al., 2004). However, the tedious nature and the difficulty in differentiating soil pores from the mineral grains, may limit its usage.

2.2. Airflow through grain bulk

2.2.1. Aeration

Aeration is often used as effective non-chemical method in the preservation of stored grains by the movement of ambient air through the stored grain bulk (Navarro and Noyes, 2002). The two prime objectives of aeration are: cooling the temperature of the grain to the ambient temperature and bringing the grain throughout the bin to a uniform temperature (Navarro et al., 2012).

Typically, the process involves using a fan to move air through perforations or duct at the bottom of the grain storage bin into the stored grain to change the grain condition. The flow of air through the grain during aeration causes the formation of three zones, with different

moisture contents and temperatures, in the grain bulk. These zones are separated by a temperature front and a moisture front as shown in the figure (2.1) (Navarro and Noyes, 2002). Zones A and B are separated by a moisture front, while the temperature front separated Zones B and C. These fronts or zones move through the bed of grains in the same direction as in airflow.

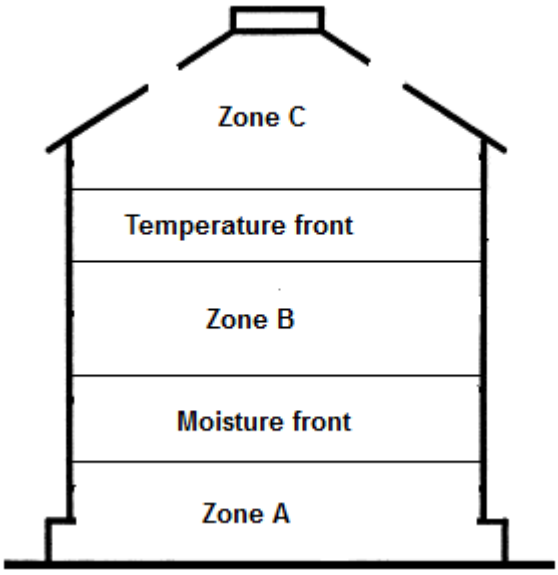

Figure 2.1: Zones in bed of aerated grain

The grain in zone B is at the dwell state, the state that will eventually prevail throughout most of a bed of aerated grains. The zone A exists at the bottom of the bin where the temperature and moisture content are in equilibrium with temperature and relative humidity of the air coming into the bin, while grain in zone C is yet to be affected. As the aeration proceeds, the zone C reduces in size and will disappear when the temperature and moisture fronts have passed through the grain bulk.

Most freshly harvested grains are high in moisture and the presence of moisture in the stored grain supports the growth of fungi, and consequently, increases the grain temperature due to biological heating caused by the micro floral growth in the grain (Montross and Maier, 2001; Montross et al., 2002). And, to suppress the growth of most insects associated with

stored grains or oilseed caused due to high grain temperature, the grains temperature should be between the ranges 16 – 20^{o}C with a relative humidity not greater than 70% (Flinn et al., 1997). Aeration has also being use for preventing moisture migration, removing of fumigant residue and odour in the stored grains.

Drying

Drying is one of the most widely used methods of food preservation (Ibrahim, 2006). Grain drying involves removing excess moisture from grains to a level that is acceptable for storage, processing or marketing (Akpinar and Bicer, 2004). Dincer and Sahin (2005) defined drying as a thermal process in which the transfer of unsteady heat and moisture content occur simultaneously. Apart from quality preservation, drying helps to reduce storage space and weight of food products during transportation (Medeni, 2001; Erkekin and Yaldiz, 2004). The commonly used drying technologies include near-ambient air drying (Jayas and White, 2003), hot air drying (Narong et al., 2012), solar drying (Basunia and Abe, 2001), microwave drying (Medeni, 2001), superheated steam drying (Tang and Cenkowski, 2000), far- infrared drying (Jun and Sheng, 2006).

The use of near-ambient air or hot air is more common for drying grain, because of their simplicity and low energy consumption (Richard et al., 1987; Jayas and White, 2003). Similar to aeration, grain drying involves the use of forced air, near–ambient air or hot air, to flow through the perforated bottom area into the grain bed with the help of a fan (Jayas and White, 2003). The rate at which moisture is evaporated out of the grain through convective heat transfer from the air to grain depends on the air temperature, initial moisture of grain, airflow rate and the grain properties (Brooker et al., 1974; Jayas and White, 2003). The hot air drying involves the addition of heat to the air to achieve the necessary drying condition (Navarro and Noyes, 2002).

However, ensuring that the moisture content of the grain is not above the required safe moisture content (Table 2.1) and storing it at cool temperatures will greatly enhance air drying methods. (Jayas et al., 1995).

Table 2.1: Upper limit of safe moisture content

Crops	Moisture Content (%) w.b
Wheat	14.5
Oats	14
Barley	14.8
Canola	10
Soybeans	14
Corn	15.5
Peas	16

2.2.2. Design of Aeration systems

2.2.2.1. Airflow resistance

The airflow resistance through the grain bulk is the most important design factor to be considered in the design of aeration systems (Navarro and Nayos, 2002). Airflow resistance through the grain bulk is affected by several factors, including grain kernel size and shape, airflow direction, airflow rate, bulk density and filling method (Rajabipour et al., 2001; Jekayinfa, 2006; Lukaszuk et al., 2008; Shahbazi, 2011; Kenghe et al., 2012).

According to the literature reviewed by Alagusunadram and Jayas (1990), many researchers have empirically determined the airflow resistance by measuring the pressure drop along the bed of the grain bulk that is being tested at different flow rates, and then fitting the experimental data obtained to an empirical or semi empirical equations for estimating the airflow resistance of the grain bulk (Rajabipour et al., 2001; Jekayinfa, 2006; Lukaszuk et al., 2008; Shahbazi, 2011; Kenghe et al., 2012). Also, some of these results have been presented as curves in the ASABE standard (ASAE D272.3, 1996). These empirical equations or

standard curves give a conservative estimate of the airflow resistance, because the effects of factors, such as, the filling method, moisture content, and bulk density on the airflow resistance are not considered (Navarro and Nayos, 2002).

2.2.2.2. Airflow rate

The airflow rate of aeration depends on the purpose of aeration, the type of grain, the type and the size of the storage structure. Foster and Tuite (1992) gave a recommendation for aeration rate for on-farm and flat storages as 1.3 (L s^{-1}) m^{-3} for corn and soybeans, and 0.7 (L s^{-1}) m^{-3} for wheat, barley and other small seed crops. For commercial bins or silos, they recommended 0.7 (L s^{-1}) m^{-3} for corn and soybeans and 0.3 (L s^{-1}) m^{-3} for wheat, barley and other small seed grains.

They explained that airflow rate for wheat in flat and deep bins were less than those for corn because of the high airflow resistance of small seed grains. Also airflow rates for flat storages were higher than the deep bins, because airflow distribution was less uniform in flat bins than in deep bins. Friensen et al. (1982) gave the airflow rates according to aeration purposes. They stated that for near–ambient air drying (combination of drying, drying, and cooling), the airflow rate should range from 1 to 2 (L s^{-1}) m^{-3}; 5 to 20(L s^{-1}) m^{-3}, 5 to 10 (L s^{-1}) m^{-3}; and 5 to 10(L s^{-1}) m^{-3} of grain respectively. The airflow rate recommended by Canadian was 1 to 2 (L s^{-1}) m^{-3} (Navarro and Noyes, 2002).

2.3. Airflow resistance through grain bulks

Forced movement of air through a grain bulk causes energy loss due to friction and turbulence, non-uniform and “tortuous” movement of air in the grain bulks, leads to drop in pressure of the moving air (Rajabipour et al., 2001; Jekayinfa, 2006; Lukaszuk et al., 2008; Shahbazi, 2011; Kenghe et al., 2012). This pressure drop is termed airflow resistance. Due to the heterogeneity characteristics of grain bulks, airflow resistance is not uniform (Navarro and

Noyes, 2002). To ensure energy efficiency in the design of systems for aeration or drying, understanding of airflow resistance is essential. The determination of airflow resistance of various grain bulks has been carried out by many researchers and the findings have been reviewed in detail by Alagusunadram and Jayas (1990) and Gayathri et al. (2007).

According to Gayathri et al. (2007) determination of airflow resistance in grain bulks are mostly experimental in nature, which typically involved the measurement of pressure drops along the bed of grain at different flow rates, and then fitting the experimental data to an empirical or semi empirical equations for estimating the airflow resistance. Shedd (1953) developed an equation to describe airflow resistance in grain bulks, by measuring the pressure drops in different beds of grain at various airflow rates. This can be seen in equation (2.4)

$$\frac{\Delta P}{L} = A_1 V^{B_1} \tag{2.4}$$

where:
$\Delta P =$ pressure drop (Pa)
$L =$ length of the grain bed in the test column (m)
$V =$ airflow rate per unit area ($(m^{-3} s\, m^{-2})$).
$A_1 \ and \ B_1 =$ constants (dependent on the type of grain).

This Shedd's model has been used by several researchers to represent the relationship between the experimental data of pressure drop and airflow rate for various grains (Madamba, 1994; Jekayinfa, 2006; Kenghe, 2012). One of the limitations of the Shedd's model is that it can only be used to predict airflow resistance over a narrow range of airflow rate (0.00056 to 0.203 ($m^3\ s^{-1}$) m^{-2}) (Navarro and Noyes, 2002). Therefore, Hukills and Ives (1955) proposed another model (equation 2.5) for a wider range of airflow rate (0.01 to 0.20 ($m^3\ s^{-1}$) m^{-2}) based on the same data used by Shedd.

$$\frac{\Delta P}{L} = \frac{A_2 V^2}{In(1 + B_2 V)} \tag{2.5}$$

where:

A_2 and B_2 = constants (dependent on the type of grain).

Although, the model by Hukills and Ives (1955) have been widely used for predicting the relationship between the pressure drop and the airflow rates for grain bulks (Jekayinfa, 2006), it did not illustrate the effect of such factors as the pore shape and size of the grain bulks. Ergun's equation (Ergun, 1952) has been widely used to describe airflow resistance in porous media. The equation (equation 2.6) accounts for the pore structure of porous medium by introducing parameters such as the particle diameter and porosity.

$$\frac{\Delta P}{L} = A_3 V + B_3 V^2 \tag{2.6}$$

where:

ΔP = pressure drop (Pa)

L = length of the grain bed in the test box (m)

V = airflow rate per unit area $(m^{-3} s\, m^{-2})$

$A_3 and\ B_3$ = viscous and the inertial term of the equation.

The viscous and the inertial term ($A_3 and\ B_3$) are defined as a function of grain bed parameters as:

$$A_3 = 150 \frac{(1-\varepsilon)^2}{\varepsilon^3} \mu \frac{1}{d^2 g} \tag{2.7}$$

$$B_3 = 150 \frac{(1-\varepsilon)^2 \rho}{\varepsilon^3 d g} \tag{2.8}$$

where:

ε = fractional porosity

d = equivalent diameter of the bed (m)

μ = viscosity of the flow fluid $(Pa.s)$

ρ = bulk density of the bed material ($kg^{-1}m^3$)

g = acceleration due to gravity (ms^{-2})

Although, Ergun's equation has been widely used in modeling airflow resistance in porous medium, Kumar and Muir (1996) and Savicki (2004) showed that Shedd's equation gave a best fit to the experimental data of pressure drop for grain bulks. Hence, many researchers have modified Ergun's equation to enhance its accuracy for prediction of airflow resistance in grain bulks (Barkker-Arkema et al., 1969; Hunter, 1983; Wu et al., 2008). Based on the effect of some notable factors such as the grain moisture content (Giner and Denisienia, 1996), the bulk density (Molenda, 2005), presence of fine or foreign materials (Haque et al., 1978), air flow direction (Hood and Thorpe, 1992; Crozza and Pagano, 2006), different empirical models for describing the relationship between pressure drop and airflow rate in grain bulks were developed.

Also, the anisotropic characteristics of grain bulks have been considered in some recent models (Savicki, 2004). Since most of the empirical models may not be valid outside the conditions under which the empirical constants were determined, the trend is gradually moving towards the development of a generalized theoretical models with a wider range of parameters (or important parameters) of grain bulks in the model (Jayas, 1990; Gayathri and Jayas, 2007).

2.4. Factors affecting the airflow resistance

2.4.1. Bulk density

The effect of bulk density on airflow resistance can be understood in relation to the bed porosity which depends on the bulk density. Studies have shown that decrease bulk density, increased the porosity of grain bulk (Nimkar and Chatttopadhyay, 2002). Porosity is the measurement of the percentage of void in the grain bulk. Shahbazi, (2011) stated that decrease in bulk density of chickpea seeds increased its percentage of void. This,

consequently, resulted in the reduction of airflow resistance through the chickpea seeds. Filling procedures also gave wide variation in bulk density and thus, affect the airflow resistance. Methods of filling grain into the bin have been shown to have a significant effect on the bulk density of grain bulk (Kumar and Muir, 1986; Lukaszuk et al., 2008).

Decrease in the bulk density results in lower airflow resistance (Shahbazi, 2011), Shedd (1953) concluded that the loose fill methods reduced airflow resistance and the packed fill methods lead to increased airflow resistance of the several grains. Kumar and Muir (1986) in their study to test the effect of filling methods on resistance to airflow of wheat and barley, concluded that for an air flow velocity of 0.077m s^{-1}, the resistance for layer filling which was similar to filling a bin with spreader was higher than end-filling that was similar to filing a bin with stationary spout by 25 to 35% for vertical airflow and 50 to 75% for horizontal airflow. They reasoned that the higher resistance to airflow for the layer filling was due to the higher bulk density. Lukaszuk et al. (2008) concluded that consolidation of grain samples by vibration resulted in about 2.2 times increase in airflow resistance compared to the test samples that was not vibrated after filling.

2.4.2. Moisture content

Using different grains, Shedd (1953) tested the effect of moisture content on the airflow resistance. He concluded that the airflow resistance for several grains tested at a given airflow rate was lower for moisture content of 20% or more, than that at lower moisture contents. That is, the airflow resistance decreased as the moisture content increased for all the grains he tested. The same similar conclusion was made by several other researchers (Pagano et al., 2000; Nimkar and Chatttopadhyay, 2002; Shahbazi, 2011; Kenghe et al., 2012). However, an opposite conclusion was stated by Peterson et al., (1971) that increase in moisture content resulted in higher airflow resistance. They observed about 25% increases in the airflow resistance as the moisture content increased from 16 to 19% corn grain.

2.4.3. Airflow velocity

A recent study carried out by Kenghe et al. (2012) on soybeans showed that the airflow resistance increased as the airflow velocity increased. Similar observation was made by many other researchers (Nimkar and Chatttopadhyay, 2002; Jekayinfa, 2006; Shahbazi, 2011). Rajabipour et al.(2001) stated that with an increase in airflow velocity from 0.12 to 0.25 m s^{-1}, the airflow resistance increaseD 3.35 times and, with an increase to 0.51 m s^{-1}, it increased 12 times. Shahbazi (2011) also stated that the pressure drop per unit length (airflow resistance) of chickpea seeds increased with increasing airflow rate in the range of 0.02 to 0.50 (m^3 s^{-1})m^{-2}. He attributed the increase in the airflow resistance of the chicken pea seeds to the increase in kinetic dissipation of the air as the velocity increased.

2.4.4. Airflow direction

Resistance to airflow in the vertical direction is generally different from that in the horizontal direction (Lai, 1980). This statement was supported by the observation by Lamond and Smith (1982) for barley. They reasoned that grain kernels lied with the major (long) axes horizontally, and this would likely lead to differences in interconnectivity between the vertical and horizontal directions. Several other investigations into this effect of airflow directions on airflow resistance showed that the airflow resistance was higher in the vertical direction than that in the horizontal direction (Kumar and Muir, 1986; Lukaszuk et al., 2008). Pagano et al., (2000) observed that the airflow resistance for oats with moisture content of 10.1% in the vertical direction was 7 to 14% higher than that in the horizontal direction. Neethirajan et al. (2008) used X – ray CT to scan the internal structure of grain bulks, and observed higher number of air paths along the horizontal air flow direction than the vertical direction.

2.5. Tortuosity of flow through grain bulk

2.5.1. Definition of tortuosity

One of the challenges of studying airflow in grain bulks is to develop a generalized airflow resistance model that correlates with the microscopic structure into the model (Gayathri and Jayas, 2007). An example is the model (Equation 2.9) developed by Kozeny – Carman(1937) for relating permeability to geometric parameters of porous media, in which the porous medium was assumed to be equivalent to a bundle of capillaries of equal length and constant cross section .

$$k = \frac{\varphi^3}{\beta\tau^2(1-\varphi)^2S^2} \tag{2.9}$$

where:

$k =$ permeability of the porous media(m^2).

$\varphi =$ porosity (decimal).

$S =$ specific surface area per unit volume of solids (m^2/m^3).

$\beta =$ constant characteristics for a particular type of porous medium.

$\tau =$ tortuosity.

Tortuosity is physically defined as the ratio of the actual microscopic path length to the length parallel to the direction of the pore channel in the porous media and mathematically expressed as (Hilmi, 2000; Bernard, 2006; Rahul et al., 2010; Arthur et al., 2011; Maciej and Zbigniew, 2012):

$$\tau = \frac{L_e}{L} \tag{2.10}$$

where:

$L_e =$ actual path length (m)

$L =$ length parallel to the direction of the pore channel(m).

While the length parallel to the pore channel can be easily measured and unambiguously specified, the actual path length is not, because in real porous media the actual flow paths are extremely complicated as the fluid paths continuously change in cross section, shape and orientation, making it difficult to identify a single path length of flow in the porous media (Maciej and Zbigniew, 2012). Hence, tortuosity is a statistical average of the many tortuous path lengths (Koponen et al., 1996).

Despite the ambiguity in the definition of tortuosity, it is generally understood as the ratio of an effective path length to the length (porous bed length) parallel to pore channel through the porous media. Boudreau (1996) proposed the following rule to serve as a guide for the definition of tortuosity.

$$\tau \geq 1 \tag{2.11}$$

This means that the actual average path followed by the fluid in the porous medium is longer than the length of the porous medium.

$$\tau \to 1 \quad as\ \varphi \to 1 \tag{2.12}$$

That is there will be no hindrance to the flow path, if there are no obstacles in the porous medium. Similarly,

$$\tau \to \infty \quad as\ \ \varphi \to 0 \tag{2.13}$$

This means that the tortuosity will become extremely high if the porosity is very small. Tortuosity is a very important microscopic property of the porous media used in many theoretical models in solving problem of material transport in porous media. Yu and Li (2004) showed in their model of airflow resistance through agricultural bulk grains that airflow resistance was related to the tortuosity value which accounts for the complex paths in grain bulks, unlike the widely used Ergun's equation which assumed, erroneously, a straight line geometry for the pore space.

2.5.2. Determination of tortuosity

2.5.2.1. Experimental Methods

There are two basic experimental methods for indirect estimation of tortuosity. The first method involves measuring a quantity termed the formation factor obtained from electric resistivity. Wyllie and Spangler (1966) assumed that the tortuosity of a porous rock can be related to its resistivity factor which is defined as the ratio of the resistivity of a porous material completely saturated with an electrolyte to the resistivity of the electrolyte itself. Using brine as electrolyte, they were able to measure the tortuosity of porous rock based on the formation factor and the porosity of the rock. For a porous medium completely saturated with brine. as follow:

$$R_b = (\rho_b)\left({}^{L}/_{A}\right) \tag{2.14}$$

where:

$R_b =$ resistance of the porous medium with the electrolyte(Ω)

$\rho_b =$ resistivity ($\Omega.m$)

$L =$ actual length (m)

$A =$ cross-section area (m^2)

And the bulk resistance of formation of brine:

$$R_w = (\rho_w)\left({}^{L}/_{A}\right) \tag{2.15}$$

where:

$R_w =$ resistance of the porous medium with the electrolyte(Ω)

$\rho_w =$ resistivity ($\Omega.m$)

Only the effective area A_e of the original area A is available for current flow along the effective length L_e

By combining equations (2.14) and (2.15) to obtain

$$R_b = (\rho_b)\left({}^{L}/_{A}\right) = (\rho_e)\left({}^{L_e}/_{A_e}\right) \tag{2.16}$$

Dividing the Eq. (2.14) and Eq. (2.15) to obtained the resistivity factor

$$F = {}^{R_b}/_{R_e} = {}^{\rho_b({}^{L}/_{A})}\Big/_{\rho_e({}^{L}/_{A})} = {}^{\rho_b}/_{\rho_e} \tag{2.17}$$

$R_e =$ resistance of the electrolyte(Ω)

Using the effective length L_e and the effective area A_e ; where $A_e < A$. Equation (2.17) can be written as

$$F = {}^{({}^{L_e}/_{L})}\Big/_{({}^{A_e}/_{A})} = {}^{\rho_b}/_{\rho_e} \tag{2.18}$$

Porosity ∅ can be defined as

$$\emptyset = {}^{L_e A_e}/_{LA} \tag{2.19}$$

From equation (2.19)

$$\emptyset = {}^{({}^{A_e}/_{A})}\Big/_{({}^{L_e}/_{L})} \tag{2.20}$$

And since tortuosity, $\tau = {}^{L_e}/_{L}$, substituting tortuosity in equation (2.18)

$$\emptyset = {}^{({}^{A_e}/_{A})}\Big/_{\tau} \tag{2.21}$$

Therefore;

$${}^{\emptyset}/_{\tau} = {}^{A_e}/_{A} \tag{2.22}$$

By combining equations (2.18) and (2.22) gives

$$F = {}^{({}^{L_e}/_{L})}\Big/_{({}^{\emptyset}/_{\tau})} \tag{2.23}$$

And since tortuosity, $\tau = {}^{L_e}/_{L}$, substituting tortuosity in equation (2.23) gives

$$F = {}^{\tau}/_{({}^{\emptyset}/_{\tau})} \tag{2.24}$$

Simplifying equation (2.24) gives

$$\tau = (F\emptyset)^{1/2} \tag{2.25}$$

Similarly, Winsauer (1952) empirically determined the tortuosity of a porous medium by measuring the resistivity factor using ionic mobility under the electrical potential gradient. He measured the distance traveled and the time taken by the ion movement through the tortuous channel under the influence of a potential difference applied between two planes. He gave the relationship between the tortuous length, and the time taken as follows:

$$L^i = m\left(\frac{E}{L}\right)t^i \tag{2.26}$$

where:
$L^i =$ lenth of the ion movement path under potential dfiference (m)
$t^i =$ time taken for the ion movement under potential difference (s)

The ionic mobility length in the absence of the porous medium is given by

$$L = m\left(\frac{E}{L}\right)t \tag{2.27}$$

where:
$L =$length of the porous medium (m)
$t =$ time taken (s)

Therefore, dividing the Equations (2.26) and (2.27) to obtained the resistivity factor

$$F = \frac{L^i}{L} = \frac{t^i}{t} \tag{2.28}$$

Tortuosity, $\tau = \frac{L^i}{L}$, substituting tortuosity in equation (2.28) gives

$$F = \tau = \frac{t^i}{t} \tag{2.29}$$

From the experimental data, Winsauer (1952) correlated tortuosity to the porosity of the porous medium as follows:

$$\tau^2 = (F\emptyset)^{1.2} \tag{2.30}$$

Garrouch et al. (2001) carried out an experiment with the four-electrode for measuring the resistivity of four different types of sandstone rock and successfully related the determined formation factor and porosity to the tortuosity values.

The second indirect method for determination of tortuosity is through the process of diffusion of fluid in porous media. This method is based on the physical principle that the diffusion of fluid through a given porous medium is affected by the microscopic channel structure of the porous medium, especially at a low flow rate. Garrouch et al. (2001) pointed out that the diffusion of fluid in porous medium was a process that depended on the geometry of the pores. The ratio of the effective bulk diffusion coefficient to the diffusion coefficient in the absence of the porous medium was related to tortuosity. Van Brakel et al. (1974) showed that apart from the porosity, the diffusivity was affected by the tortuosity and the constrictivity factor. They explained that the tortuosity factor accounted for the non parallel pore space segment in the porous medium while the constrictivity factor accounts for variation along the segment given as:

$$Q = {}^{D_e}/_{D} \tag{2.31}$$

where:
$Q =$ diffusivity
$D_e =$ effective diffusion coefficient $(m^2 s^{-1})$
$D =$ diffusion coefficient $(m^2 s^{-1})$

Hence, diffusivity was developed as:

$$Q = \frac{\emptyset\delta}{\tau^2} \tag{2.32}$$

where:
$\delta =$ constrictivity

Recently, several other experimental methods have been used in the determination of tortuosity. Fabrizio et al. (2011) used the thermo-diffusion cell for the determination of molecular diffusion coefficient, which consequently was used for estimating the value of the tortuosity of the porous media. A temperature difference was applied to the porous medium in the thermodiffussion cell, while its refractive index was measured by means of a Mach-Zechnder interferometry. Thus, the mass diffusion coefficient of the sample within the porous medium was deduced. The tortuosity of the porous medium was estimated by knowing the value of the diffusion coefficient in the free medium and relating it with the diffusion coefficient of the porous medium as follows:

$$D^* = {}^{D}/_{\tau^2} \tag{2.33}$$

where:

D^* = molecular diffusion coefficient in porous medium($m^2 s^{-1}$)

D = molecular diffusion coefficient in free medium($m^2 s^{-1}$)

τ = tortuosity

Gas diffusion nuclear magnetic resonance (NMR) has been used for estimating tortuosity of porous media (Rigby and Gladden, 1996; Mair et al. 2001; Wang et al. 2005). Wang et al. (2005) presented the measurement of tortuosity of a variety of rock samples using NMR to monitor the inflow of thermal xenon into the rock core and then calculating the time-dependent diffusion coefficient. Mair et al. (2001) utilized Pulsed Gradient Spin Echo NMR measurements of time-dependent diffusion coefficient of xenon gas filling pores of beads, for further measurements of pore surface-area-to-volume ratio and tortuosity.

Experimental data for determination of tortuosity have been obtained by the measurement of effective conductivity (Barrande et al., 2007; Garrouch et al., 2001), Berrande et al. (2007) determined tortuosity from conductivity measurements on different porous media

filled with an electrolyte (Sodium chloride solution) and comparing them with the conductivity value of the porous media without electrolyte as follows:

$$\sigma_{eff} = {\sigma^0 \epsilon}/{\tau} \tag{2.34}$$

where:

σ_{eff} = effective conductivity of the porous medium($\Omega^{-1} m^2 mol^{-1}$)

σ^0 = conductivity of the porous medium filled with electrolyte($\Omega^{-1} m^2 mol^{-1}$)

ϵ = fraction of the liquid-filled cross section of the porous medium

τ = tortuosity

Image processing techniques have been used for the estimation of tortuosity value of porous media (Gommes, 2009). Mota et al. (1999) used image analysis to determine the porosity and tortuosity of the bed structure developed from a two-dimensional simulation of packed beds composed of binary and ternary particles mixture. Neethirajan et al. (2008) employed the used of X-ray CT in scanning the internal structure of barley, pea, and using image processing techniques for estimating tortuosity by reconstructing the length of flow paths in the grain bulks. Fellah et al. (2003) proposed reflected wave propagation as another indirect method for measuring the tortuosity of porous media. The technique is based on measurement of reflected wave from a slab of rigid porous material at oblique incidence.

Apart from the fact that all the experimental methods that have been used so far for the determination of tortuosity have only indirectly estimated tortuosity value either by measuring property such as porosity of the porous medium and then relating the measured property to the tortuosity value. Although, the electrical resistance indirect experiment methods for determination of tortuosity did not consider the effect of shape of the channel on the fluid flow, which definitely in real situation will affect the movement of the fluid in the porous media (Suman and Ruth, 1993). Other limitations are that the indirect experimental methods are time consuming, complex, and are designed for a specified porous medium (Lihua and Chen, 2007).

2.5.2.2. Theoretical Methods

Theoretical methods for the determination of tortuosity are based on the use of models to portray the structure of the porous medium and flow behavior in the medium. A simple model is a collection of randomly oriented capillaries through a solid body, which was used by Peterson (1958) and Dykhuizen et al., (1989) respectively to estimate the value of tortuosity:

$$\tau = \sqrt{2} \; ; \; \tau = \sqrt{3} \tag{2.35}$$

A More realistic model was developed by Kaponen et al. (1998) in their study of creeping flow of Newtonian incompressible fluids. They used lattice gas simulations in 2D media to construct porous media consisting of randomly placed rectangles of equal size, with unrestricted overlap. They obtained a correlation between the average tortuosity (τ) and the porosity (φ) as follow:

$$\tau = 0.8(1 - \varphi) + 1 \tag{2.36}$$

Similarly, Tomadakis and Sotirchos (1993) used random walk simulation results to estimate tortuosity as a function of porosity. Yu and Li (2004) used a simple geometry model to estimate the tortuosity of flow path as a function of porosity. In their later work they proposed three different models for tortuosity in three-dimensional porous media constructed with spherical, cubic and plate–like particles by assuming that some particles overlapped unrestrictedly (Yun et al., 2006). Other theoretical methods that relate tortuosity to the porosity for different porous media are shown in Table 2.2.

Several numerical methods have been used for the estimation of tortuosity, including the fractal techniques. For example, Li and Yu (2007) used the fractal technique to estimate tortuosity of flow path through a seipinki carpet. Koponen et al., (1996). Arthur et al., (2011), and Maciej and Zbigniew (2012) used a lattice-gas simulation method for estimating tortuosity by averaging the streamlines of low Reynolds number flow in a two-dimensional matrix formed by

randomly placed, fully overlapping rectangles and squares. Wojciech et al., (2012) used the discrete element method to predict tortuosity of airflow through porous beds consisting of randomly packed spherical particles. Most of the theoretical methods are based on highly idealized structure of porous media (Lihua and Chen, 2007).

Table 2.2: Some empirical models for tortuosity of porous media

Model	Adjustable parameters	References
$\tau = 1 + Pln(\frac{1}{\varphi})$	P=0.41	Comiti and Renaud (1989)
$\tau^2 = \varphi + B(1-\varphi)$	B=0.9	Iversen and Jorgense (1993)
$\tau^2 = 1 - Cln\varphi$	C =2	Boudreau (1996)
$\tau = 1 + a\frac{(1-\varphi)}{(\varphi-\varphi_c)^m}$	a=0.65 and m=0.15	Koponen et al. (1997)

2.6. Flow visualization

2.6.1. Introduction to flow visualization

Flow visualization has played an important role in understanding, analyzing, developing and evaluating fluid flow processes; investigating the characteristics of the flowing fluids, and providing quantitative data for further computational investigations (Merzirch, 1974). One of the famous flow visualization techniques was used by Reynolds, he studied laminar-turbulence transition in pressure driven pipe flow (Merzirch, 1974).

Flow visualization techniques generally aim to alter the fluid in a way that the fluid transport can be detected without distorting the fluid motion (Yu et al., 2005). The velocity field, and area and shape of flow path are some of the many results that can be obtained from flow visualization (Merzirch, 1974). Generally, flow visualization techniques can be classified into three: tracer methods, optical methods, and energy transfer methods.

2.6.2. Methods of flow visualization

2.6.2.1. Tracer Methods

This method involves the introduction of visible tracer materials into the flowing fluid. It is regarded as an indirect method because the motion of the fluid is being inferred from the motion of the tracer particles (Adrian, 1991). However, the difference between the flow of the tracer material and the fluid can be minimized by using tracer materials that have approximately the same density as the fluid. Using tracers for flow visualization can give excellent results for steady state flow situations, but unreliable results for unsteady state, if differences in the thermodynamic properties of the tracer material and the flowing fluid exist (Merzirch, 1974; Leweke, 2012).

A common type of tracer is dye that has been used in visualization of liquid flow. Buchgraber et al. (2012) used a dye tracer for the visualization of preferential flow of water and solute transport in soil. Flurry (2003) applied a dye tracer in hydrology studies in the vadose zone of soil. Flow visualization using dye is an inexpensive, easy-to-implement technique, which gives rapid quantitative assessment of fluid flow (Nunata et al., 2012). However, using dye for flow visualization may cause an inevitable disturbance to the flow pattern, and also it is difficult to control the injection of dye into the flowing fluid (Nunata et al., 2012)

Smoke is another example of tracers for visualization of gas flow (Peter, 1993). Visualization of airflow by using smoke tracers was reviewed in detail by Mueller (1983). Using smoke tracers requires a generating source for the production of the smoke. Smoke may be

generated by burning materials such as wood or tobacco to vaporize mineral oil, producing mist as a result of reactions of various chemical substances or condensing steam to form a visible fog (Yu et al., 2005).

Smoke tracers have been used for visualization of many airflow processes in recirculating wind tunnel (Yu et al., 2005; Wolfram et al., 2008). Also, it has been used in studying airflow distribution through the microstructure of soil (Yu et al., 2005). Another important tracer method is the use of suspended anisotropic particles such as aluminum or lycopodium. The particles align in the liquid flow in such a way that in parallel light the vortices will appear bright (Savas, 1985). Proper lighting is important in order to enhance visualization of the fluid flow when tracers are used for fluid flow visualization (Wolfram et al., 2008). Jasmine (2000) used strobe lamps to enhance smoke visualization of the flow-field created by a flapping micro-air vehicle (MAV).

2.6.2.2. Optical methods

Optical methods maybe used for visualizing the movement of fluids which have non-uniform density. The methods are based on the fact that the refractive index of fluids is a function of density, pressure or temperature of the flowing fluid; therefore the flowing fluid can be made visible by using optical methods that are sensitive to changes in the refractive index. Optical visualization methods are generally very complex (Astarita et al., 2006). However, they are more advantageous than the tracer methods because they are purely non-disturbing. There are three optical techniques that have been used for flow visualization, namely shadowgraph, Schlieren photography, and interferometric methods (Peter, 1993). The shadowgraph method involves passing a monochromatic light beam through the flowing fluid, and an optical device behind the flowing fluid then records non- uniform illumination, which reflect the changes in fluid density, temperature or pressure.

Optical technique for flow visualization was first used by Woodcraft et al., (1999) to study the Rayleigh-Bernard convection in liquid helium. Several other researchers used the optical techniques for visualization of fluid flow (James et al., 2005; Falk et al., 2012). The Schlieren optical method involves deviation of a parallel illuminating light by variation in the refractive index of fluid, and the resultant deflection angle is proportional to the refractive index gradient and to the light path length (Peter, 1993; James et al., 2005; Falk et al., 2012).

An extended light source is needed in Schlieren photography and also the optical arrangement is different from the arrangement used in shadowgraphy (Ohyama et al., 2007; Falk et al., 2012). Schlieren optical methods have been successfully used for the investigation of production and motion of shock waves in super fluid helium (Ueta et al., 2002). Both shadowgraphy and Schlieren methods require calibration in order to obtain quantitative information about the refractive index of fluid (James et al., 2005).

The Interferometric method involves passing parallel light from a monochromatic source through a complex mirror arrangement, before entering the flowing fluid and the density variation of the flowing fluid is then depicted on the plane. Lida et al. (1996) used laser holography interferometry to depict virtually thermal wave in super fluid helium. Other optical methods for flow visualization include infrared thermograph (Giovanni et al., 1998; Astarita et al., 2006), magnetic resonance imaging (Ashvin et al., 2011), and digital imaging (McGregor et al., 2008).

2.6.2.3. Energy transfer methods

The energy transfer method involves the transfer of energy to a portion of the flowing fluid to induce density variation in the fluid, which can then be visualized by any of the optical methods. The density variation can also be observed directly without using the optical techniques, depending on the degree of luminosity of the flow caused by transfer of energy

and how fast the fluid is flowing (Merzirch, 1974). This method is mostly used for visualizing the flow of compressible fluid. The flow of the fluid is governed by supersonic or hypersonic speeds at low average density below the range of sensitivity of most optical methods (Merzirch, 1974). The method is based on the collision of electrons provided by an electron beam or by an electric discharge with the molecules of the fluid to produce a luminous signal depending on the local fluid density.

This signal can then be visualized directly or by using an optical method. Flow visualization by using electron beams was first reported by Schumacher (1952). Several other studies have been carried out for visualization of flow of air (San, 1982), as well as nitrogen and helium. In addition to qualitative visualization of flow, the energy transfer by using electron beams or electric discharge may also serve for quantitative measurement of flow temperature and density (Merzirch, 1974).

3. MATERIALS AND METHODS

3.1. Materials

3.1.1. Test box (bin)

A transparent rectangular box (27 × 25 × 2 cm) made of 1.6 cm thick Plexiglas was designed and constructed to conduct the experiments. The test box was designed to have a small thickness (2 cm) to simulate 2 D test box flow and permit effective visualization of the smoke movement in the box (figs.3.1 and 3.2). A similar box design was used for studying air flow through visualization by Carl and Craig, (1999) and Peterson et al., (2000). The box had a perforated bottom with 1cm diameter holes spaced at 1cm for introducing air into the grain contained in the box. The box sat on a plenum (25 × 15 × 9 cm) that was used for the introduction of the smoke into air stream (fig.3.2).

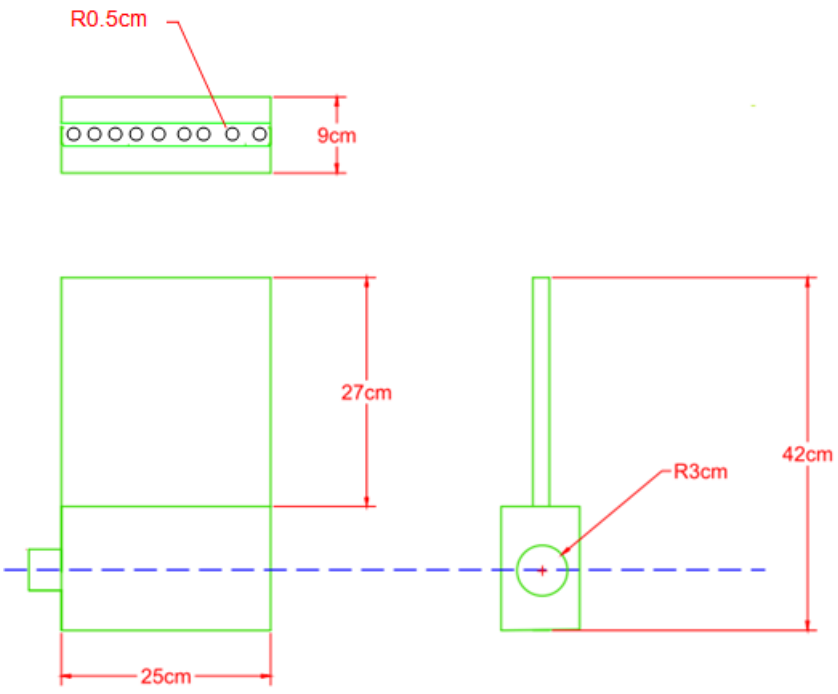

Figure 3.1: Isometric projection drawing of the test box

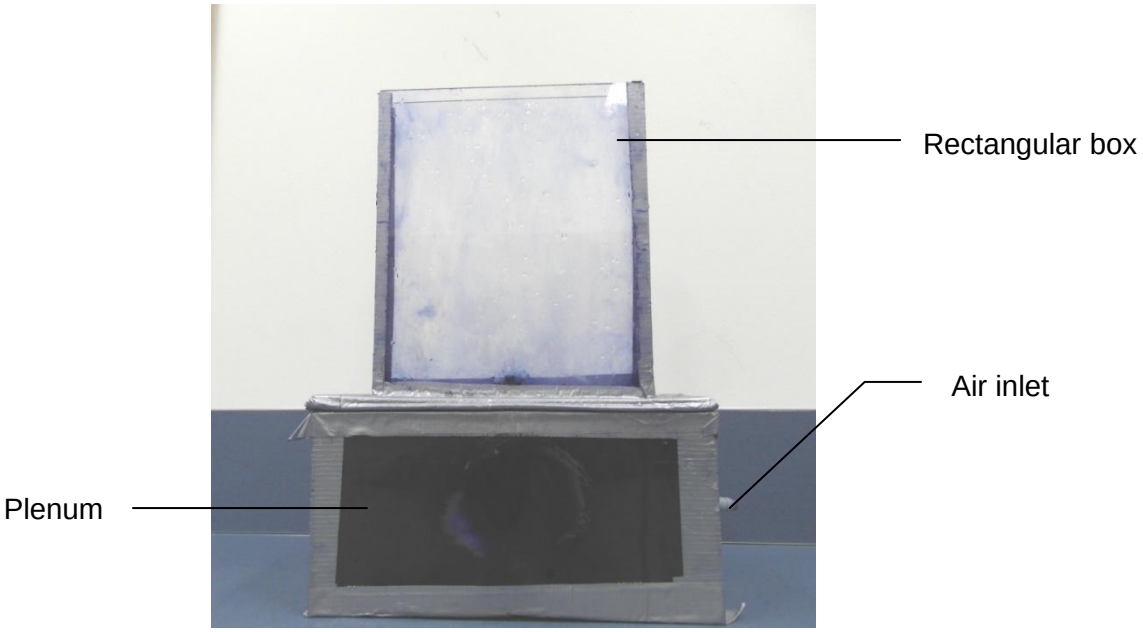

Figure 3.2: Test box

3.1.2. Airflow visualization and measurement

A centrifugal fan (Model -59999C 4DColeman Quick Pump, Sunbeam Corp. Ltd., Brampton, ON, Canada) was used to supply the required airflow. The airflow rate was controlled by using both a fan inlet restriction and an in-line micro control valve. A PVC pipe of 65mm i.d was used for channeling the air into the plenum, and the airflow rate was measured by using a bubble flow meter (Model – M30, Mini Buck, A.P.Buck Inc., Orlando, FL, USA). The flow meter had an accuracy of $\pm$0.5%.

3.1.3. Colored smoke cartridge

The Regin smoke cartridge S102 (b) 18gr blue color smoke, manufactured by Regin HVAC Product, Oxford, CT, USA, was used for the visualization of air flow (fig.3.3). The cartridge produced non–toxic smoke with particle sizes of 0.3-2.5 microns, and it does not leave behind any residues. Selection of this smoke cartridge was based on the visibility of smoke when injected into the air flowing through the grain bulk and also the density of smoke produced

was approximately the same density as air. Different colors were tested and the blue smoke was selected because it was most visible in soybeans used for this study.

Figure 3.3: Smoke emitter cartridge

3.1.4. High Speed Camera

A high speed camera (Exilim EX-F1 Casio Computers Co., Ltd, Tokyo, Japan) was used for recording the movement of the smoke in the test box filled with grain. The camera had a 12x zoom Lens, with focal length ranging from f/2.7 to 1/15 and ISO 100 to1600, capturing up to 1200 frames per seconds and about 60fps rate at full resolution (512 × 384). For all the experiments this camera was mounted on a highly stable tripod (Slik Pro 700DX, Model – 8330T, Slik Cooperation, Hidaka, Japan).

3.1.5. Physical properties of the test grain

The grain tested in this study was soybeans. The moisture content of the soybean samples was determined by the standard oven method using temperature setting at 105^0C for 72 hours as outlined in ASABE R2008 S352.2 (ASABE, 1998).

Three samples of 15 g each were placed into aluminum dishes having a diameter of 0.055 m and height of 0.015 m. The dishes with grain samples were weighed by using an

electronic precision balance (CH-8606, Metter Instrument, Zurich). Then, the uncovered dishes were placed into an oven (Thelco Inc. Georgia, AT, USA). After the time elapsed, the samples in dishes were transferred to desiccators to be cooled to the room temperature. The moisture content was calculated from the initial and the final mass and expressed in percentage wet basis.

Fifty (50) soybean kernels were randomly selected for size measurement. The length, width and thickness of each kernel were measured by using a veneer clipper. The surface area was calculated using equation 3.1 (Rumsey, 1981).

$$S_W = 0.05\pi W^2 \left(1 + \frac{L^2}{W\sqrt{L^2 - W^2}} sin^{-1} \frac{\sqrt{L^2 - W^2}}{L}\right) \quad (3.1)$$

where:

$L =$ average length of the grain(m)

$W =$ average of width of the grain(m)

$S_W =$ surface area of the grain(m^2)

The average volume of the grain kernel was measured by the water displacement method. The samples were placed in a scaled tube filled with water, and the volume of the grain kernels was obtained from the displacement of water. Once the average volume of the grain kernel was obtained, the equivalent diameter was calculated from the equation 3.2. (Mohsenin, 1986)

$$D_w = \left(\frac{6V_w}{\pi}\right)^{1/3} \quad (3.2)$$

where:

$D_w =$ equivalent diameter of the grain kernel(m)

$V_w =$ volume of the grain kernel(m^3)

The sphericity of the grain was obtained using the following equation 3.3 (Rumsey, 1981)

$$\varphi_w = \frac{6V_w}{D_w S_w} \quad (3.3$$

where:

φ_w = the obtained sphericity of the soybean grain kernel

The average mass of fifty (50) soybean kernels was obtained by using a digital electronic balance with an accuracy of 0.001g. The particle density (ρ_p) was calculated from ratio of the average mass to the average volume (V_w). The bulk density (ρ_b) of the grain in the test bin was obtained from the total mass of the grain in the test bin, divided by the volume occupied by the grain in the test bin. Finally, the porosity was calculated from the particle and bulk densities as follows (Neale and Messer, 1976)

$$\emptyset = 1 - \frac{\rho_b}{\rho_p} \times 100 \quad (3.4)$$

where:
$\emptyset =$ porosity of the grain bulk
$\rho_b =$ bulk density($kg\ m^{-3}$)
$\rho_p =$ particle density($kg\ m^{-3}$).

3.2. Experimental Procedure

Flow visualization with the use of smoke is one of the simplest techniques to achieve a visual presentation of flow movement. This technique was used in this study to visualize the air flow pattern in grain bulk. It involves some main steps which include: generating the smoke, introducing the smoke into the airflow, illuminating the smoke, and photographing the resulted flow pattern.

A preliminary experiment was carried out with the use of a fog machine to generate the smoke. However, it was observed that the flow patterns were difficult to detect with

photographic equipment and the white color smoke produced by the machine gave a low contrast with the grain kernels. Therefore, a color smoke cartridge (Regin HVAC Product, Oxford, Conn., USA) was chosen used for this experiment.

The color smoke was introduced into the air flow in the plenum and then it was channeled into the text box after opening the inlet valve. The movements of the smoke were illuminated with the use of 50W halogen lamps clamped on a tripod stand placed 10-cm distance in front of the test box and a high speed camera (Exilim EX-F1 Casio Computers Co., Ltd, Tokyo, Japan) set to 60 frames per seconds with 3.2 focal length on a manual focus for clarity (fig.3.4).

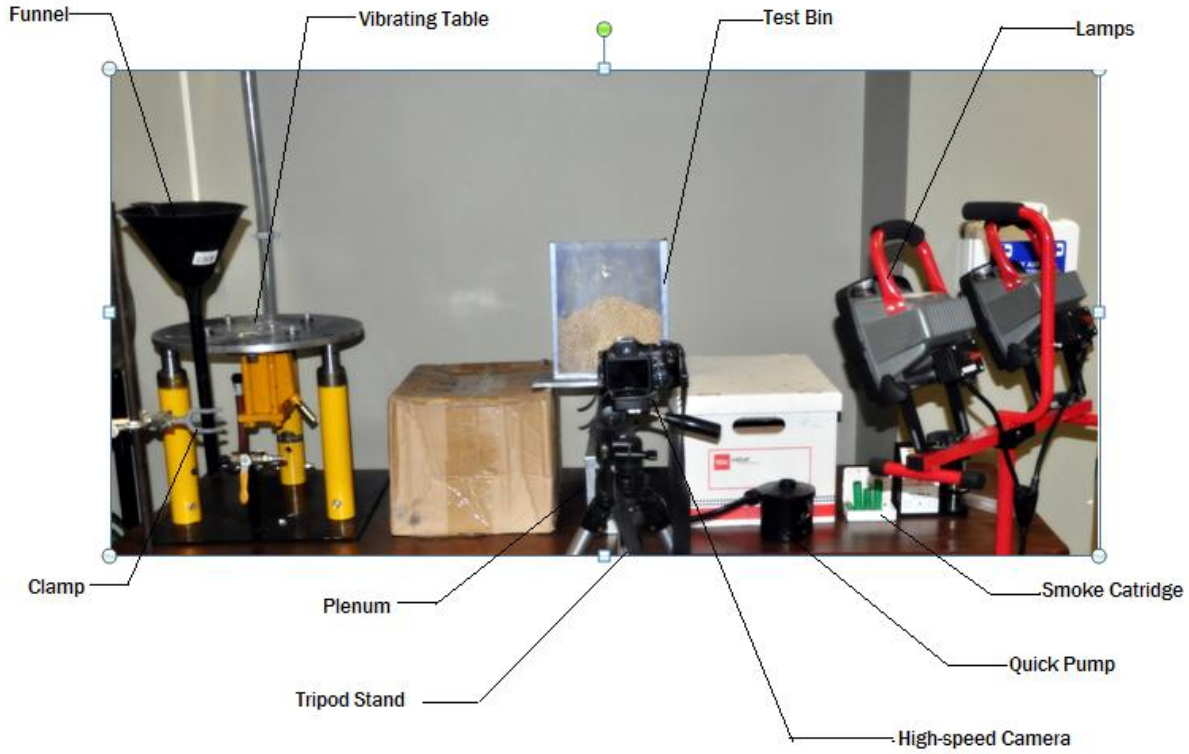

Figure 3.4: Photograph of experimental set-up

3.2.1. Filling test box

The effects of fill density on tortuosity and flow velocity were studied by using two different methods of filling soybeans into the test box (loose and dense fill). A loose fill was

accomplished by using a funnel that was placed 20 cm from the top of the test box. In this case, the grain developed a heaped surface after filling (fig.3.5).

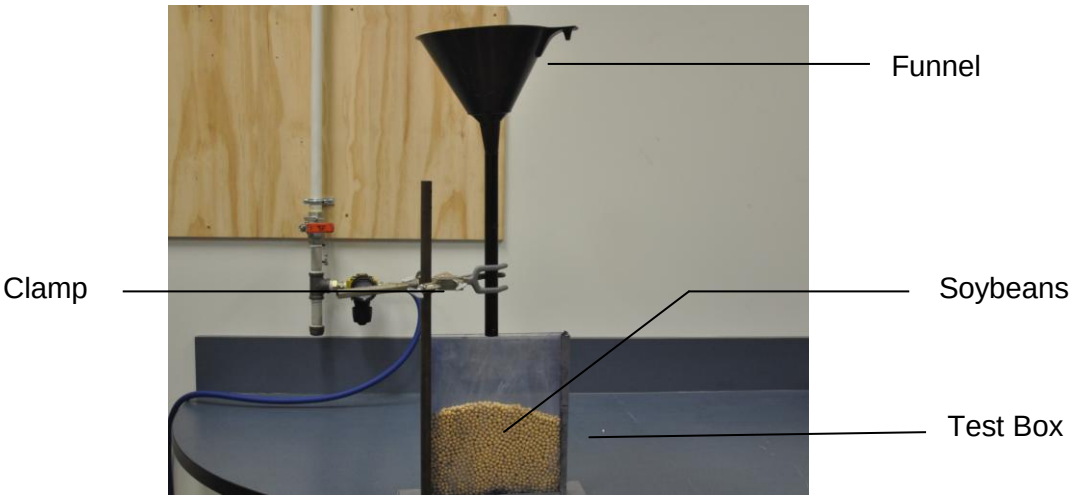

Figure 3.5: Filling soybeans into the test box to achieve loose fill

The dense fill method was achieved by vibrating the test box after filling with the funnel. The test box was placed on a vibrating table and was shaken for 30 seconds with amplitude of 0.623 mm (fig. 3.6).

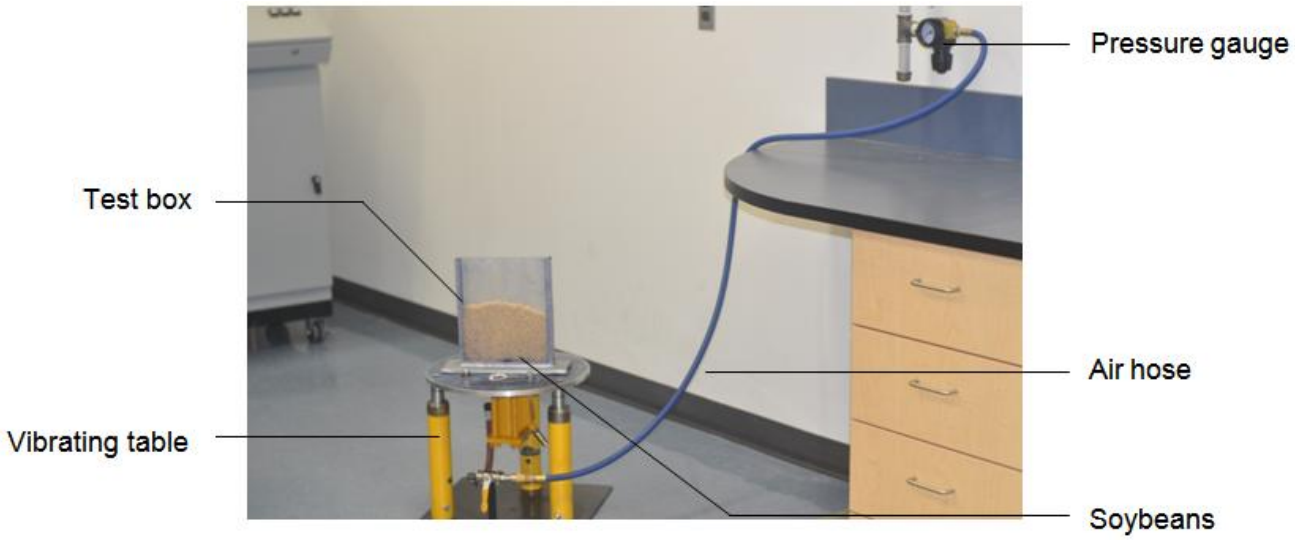

Figure 3.6: Vibrating the test box after filling to achieve dense fill (vibrating table was driven by compressed air).

This method of fillling was used to simulate the actual filling method of grains in large storage bin. This filling method was used for all the test conducted to acheive consistency in filling grains into the test bin.

3.2.2. Airflow rates

To study the effect of the flow rate on airflow path, three airflow rates (0.25, 0.45, and 0.60 $L\ s^{-1}$) were tested. A range of flow rates were tried in preliminary tests and these rates was chosen to ensure efficient flow of smoke through the soybeans bulk, with the consideration of the capacity of the fan used 0.60 L s^{-1}.

3.2.3. Image analysis

The high quality videos of smoke movement through the grain bulk were first separated into frames using commercial software of VirtualDub (Virtualdub, Quebec, Canada) (fig. 3.7). And the individual frames were then analyzed for flow paths (fig. 3.8).

Figure 3.7: Examples of image frames from a video.

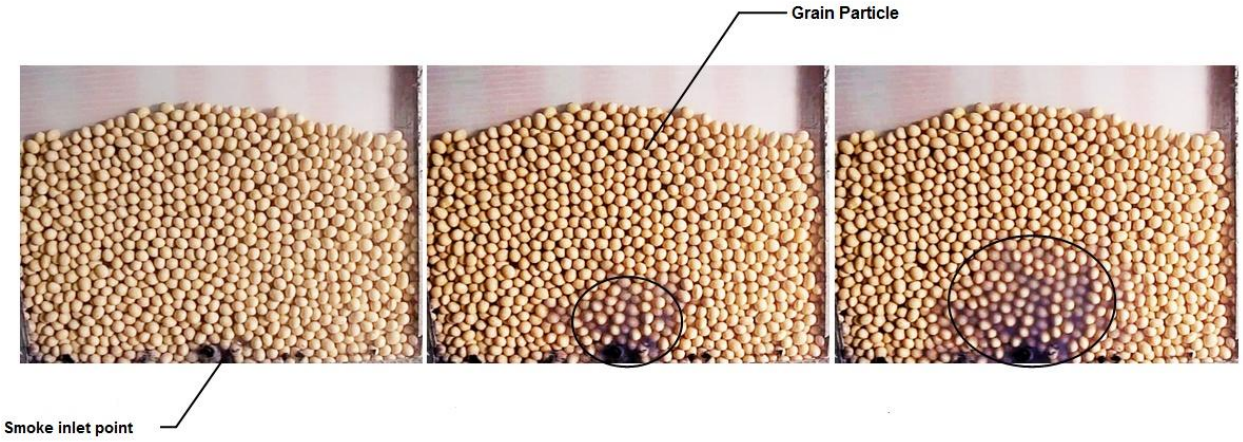

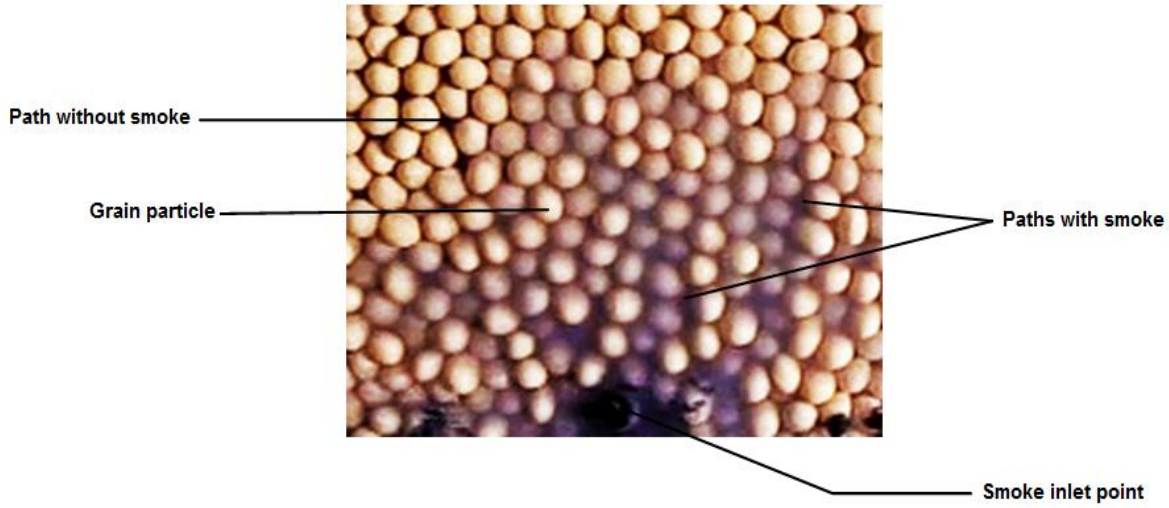

Figure 3.8: Smoke movement through the porous path in the grain bulk.

Frames image files of 512× 384 pixel RGB were extracted from the recorded videos and read into the ImageJ image processing software, a public domain Java-based image processing software(NIH, Bethesda, MD, US.). The images were combined in the ImageJ to form an image sequence (fig.3.9). This was the compilation of the images from one particular recoded video of the smoke movement in the grain bulk.

Figure 3.9: RGB Image sequence

The images were then analyzed first by subtracting a background image of the grain bulk taken before the smoke was introduced (fig.3.10). It should be noted that this background image was obtained with the same field of view and camera settings as for images of smoke flowing through the grain bulk.

Figure 3.10: RGB Background Image

Before subtraction, the background image and the image sequence were converted into 8-Bit images (figs. 3.11 and 3.12). And then to inverted images to enhance the subtraction process in ImageJ (figs. 3.13 and 3.14).

Figure 3.11: 8-bit Image sequence

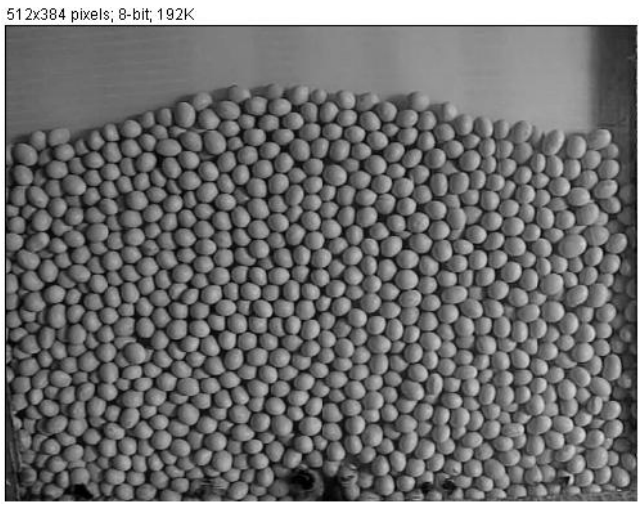

Figure 3.12: 8-bit Background Image

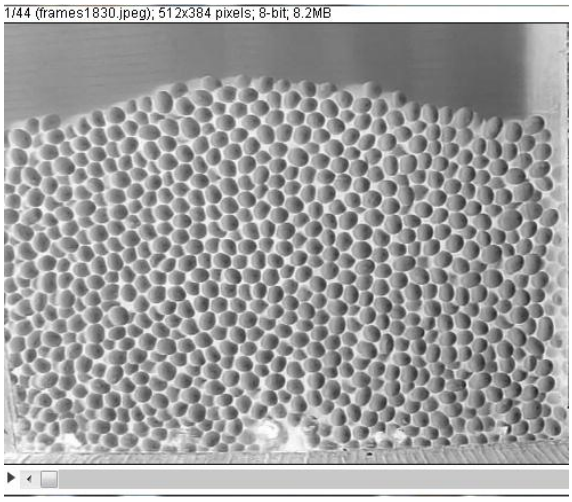

Figure 3.13: Inverted image sequence

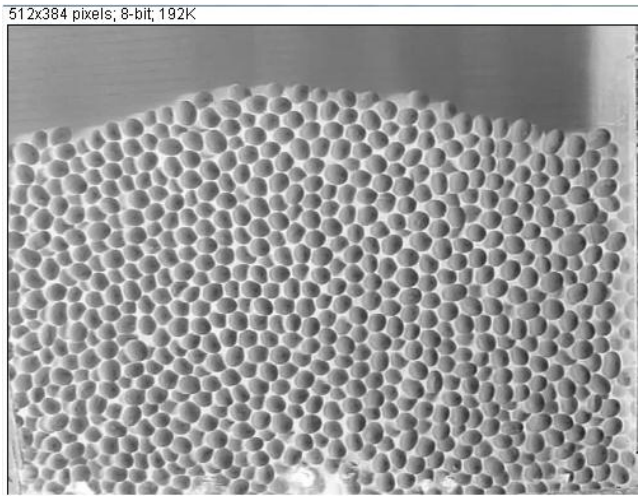

Figure 3.14: Inverted background image

Subtraction of the background image from the image sequence produced a new image sequence that showed only the smoke (fig. 3.15).

Figure 3.15: Subtracted image sequence

To track the smoke movement, the subtracted image sequence was then thresholded to further separate the flow of smoke from the grain itself and other image artifacts, creating binary images with intensity value of 1 (white) for the smoke and 0 (black) for other objects in the image (fig. 3.16).

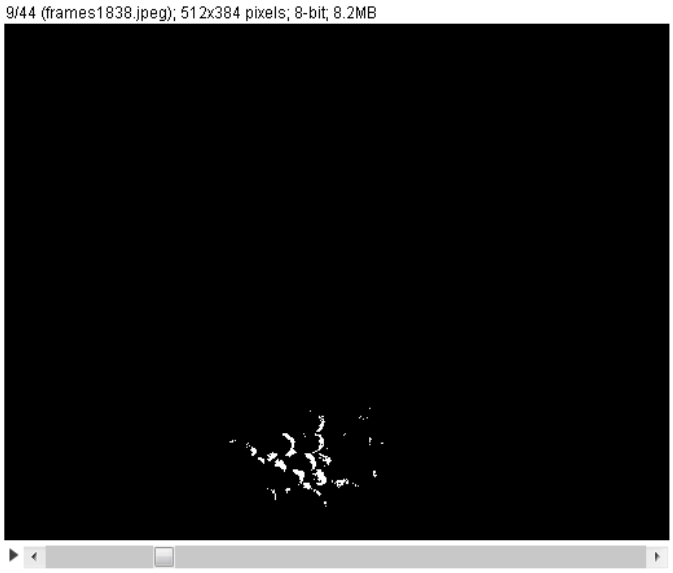

Figure 3.16: Thresholded image sequence

The smoke (flow) paths were then traced using the ImageJ manual tracking plug-in. Tracing started from the point at the bottom of the test box where the smoke was introduced to a horizontal line drawn on the image sequence 9.2 cm from the bottom of the test box (fig.3.17). The bar scale function in the ImageJ was used for converting the image pixels to the actual size of the test box, resulting in a scale of 20.401pixel cm^{-1}.

The length of each airflow path was measured and tortuosity was obtained by dividing the measured length of the air flow path by the bed thickness (9.2 cm). The average tortuosity was obtained by taken the average of the tortuosity of the flow channels. The velocity of airflow was obtained from the distance traveled by smoke between two consecutive frames, divided by the time interval between the two consecutive frames (1/60s).

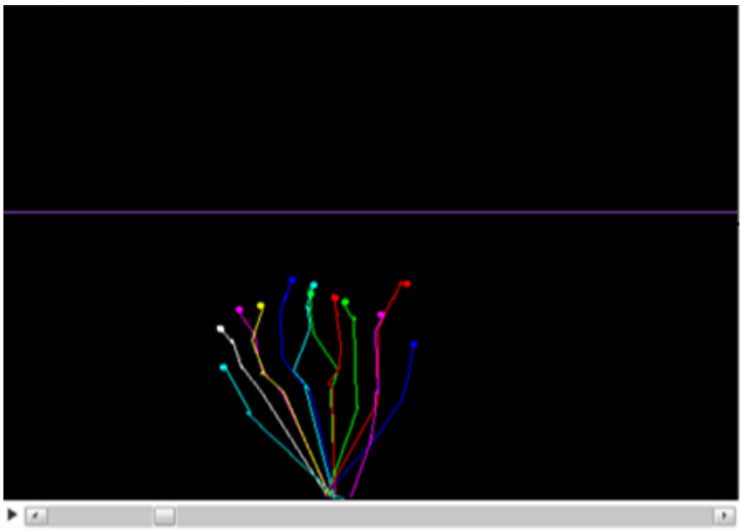

Figure 3.17: Tracked thresholded image sequence

3.2.4. Statistical Analysis

Analysis of variance was carried out with SAS statistical software (Statistical Analysis Systems, Cary, NC) to test for the effect of the airflow rate and the filling method on tortuosity and the flow velocity.

4. RESULTS AND DISCUSSION

4.1. Physical Properties of Soybeans Tested

The measured physical properties of the soybeans used in this study are shown in Table 4.1. The property values were similar to those reported by Kibar and Ozturk (2008) and Kenghe et al. (2012) at a moisture content of 8.0 and 8.7% respectively.

Table 4.1: Physical properties of Soybean grain sample (n = 50)

Moisture Content (%)	8.82	Sphericity	0.7
Average Length(m)	6.2×10^{-2}	Average mass of kernel(kg)	2.2×10^{-4}
Average Volume (m^3)	$2.14\ x10^{-7}$	Particle Density(kg/m^3)	1028
Equiv. diameter(m)	6.9×10^{-2}	Porosity (%)	39†

† Loose fill (without vibration)

4.2. Fill density and pore structure

The bulk density obtained by vibrating the test box after filling with a funnel (dense fill) was 755 Kg m^{-3} and the bulk density for the direct funnel filling (loose fill) was 632 Kg m^{-3}. The results of the bulk densities obtained for three replications for the loose and dense fill respectively is illustrated below (fig. 4.1).

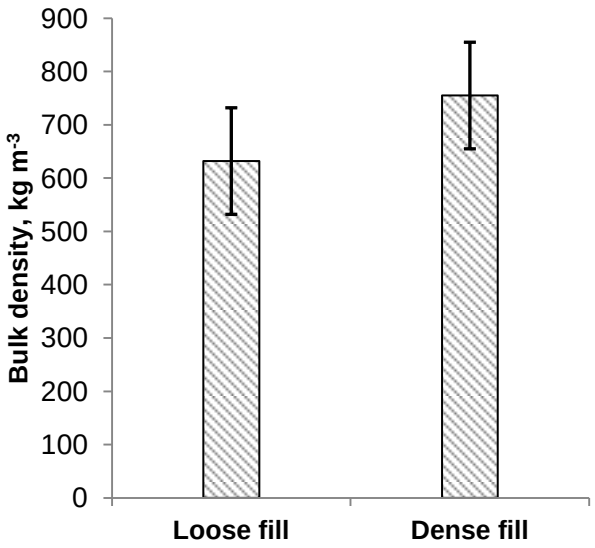

Figure 4.1: Bulk density of loose and dense fill (Error bar =standard deviation)

As the grain bulk became denser, the pore space reduced. The images taken before and after vibration showed that vibration affected not only the bulk density, but also the pore structure of the grain bulk (fig.4.2).

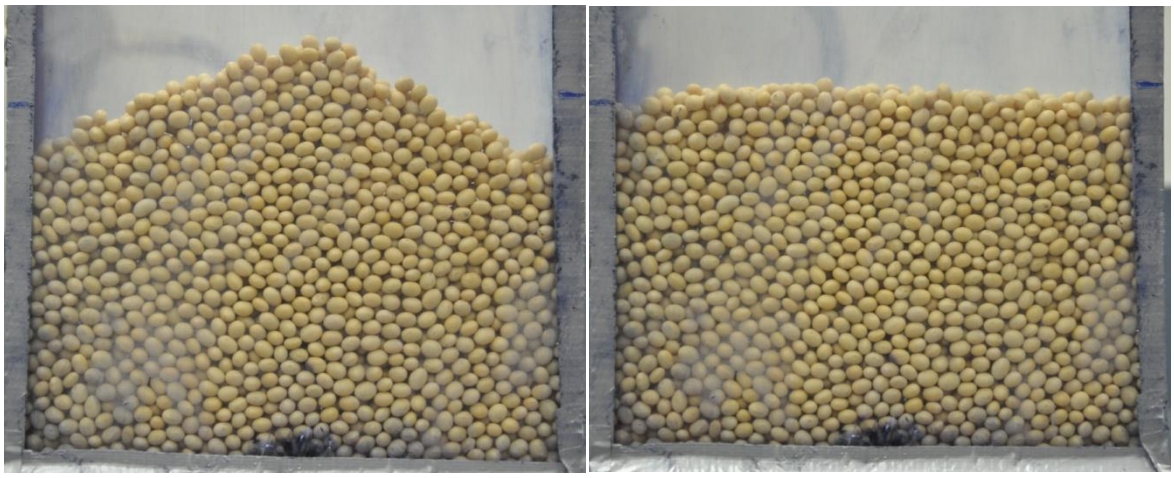

(a) (b)

Figure 4.2: Photographs of grain bulk for (a) loose fill and (b) dense fill

From the thresholded images of the loose and dense fill, the total area of airspace (void) was measured (fig 4.3). The variation of airspace along the grain bed depth for both the loose fill and dense fill was examined. It was apparent that the mean airspace of loose fill was higher than the dense fill. For the loose fill, airspace was 0.041 cm^2 $\pm$0.009, and 0.02 cm^2 $\pm$0.007 for dense fill. It was also observed that the airspace increased from the bottom to the top of the test box (fig.4.4).

These same observations were made by many other researchers (Chang et al., 1983; Neethirajan et al., 2008). Chang et al. (1983) showed that filling methods had a significant effect on the bulk density. Neethirajan et al. (2008) concluded in their study for the investigation of 3D geometry of bulk wheat and pea pores using X-ray computed tomography that change in bulk density affect the pore size and volume inside the grain bulk.

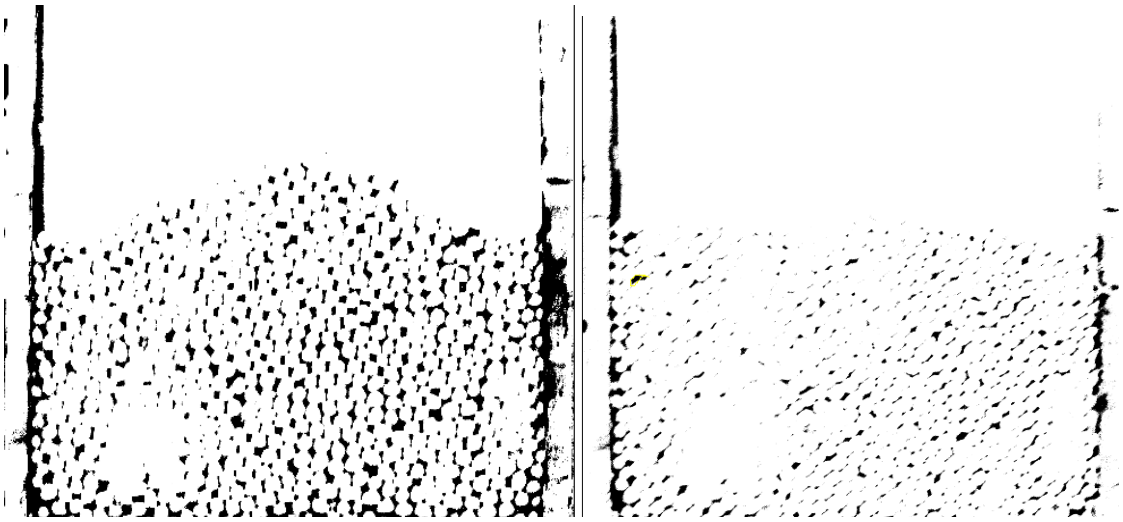

(a) (b)

Figure 4.3: Thresholded images of (a) loose fill and (b) dense fill

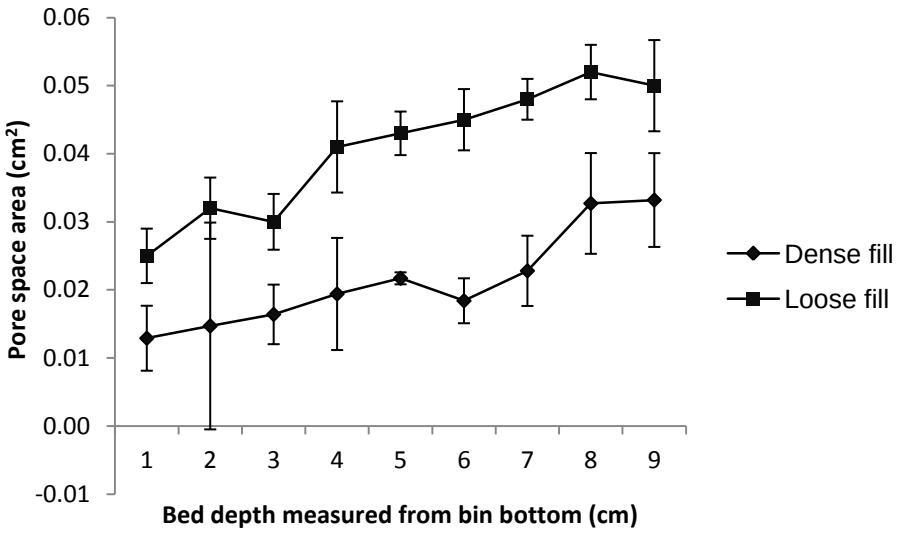

Figure 4.4: Distribution of pore space (area) along the bed depth for loose and dense fill.(Error bar = Standard deviation).

From the thresholded images of the loose and dense fill, fragmentation index which is an index of inter connectivity of airspace inside grain bulks, was calculated based on the ratio of the areas and perimeters of pores inside the grain bulk before and after dilation of the thresholded image (Hahns et al., 1992; Neethirajan et al., 2008).

$$FI = \left(\frac{P_1 - P_2}{A_1 - A_2}\right) \tag{4.1}$$

where:
$FI =$ fragmentation index
$P_1 =$ pore space perimeter before dilation (pixel)
$P_2 =$ pore space perimeter after dilation (pixel)
$A_1 =$ pore space area before dilation (pixel^2)
$A_2 =$ pore space area before dilation (pixel^2)

A lower fragmentation index signifies better connected pore channels (air path), while a higher value of fragmentation index signifies disconnected pore channel. The calculated fragmentation index was 0.56 $\pm$0.05 for the loose fill, and 0.71 $\pm$0.04 for the dense fill. This

means that pore channels inside the dense fill grains were more disconnected than the pore channels inside the loose fill grains (fig.4.5).

In other words, vibrating the test box increased the number of disconnected pore channels inside the grain bulk. For both the loose and dense fill, disconnected pore channels were higher in the middle of the grain bed (fig.4.5). This trend contradicts the fact that grain bulk will have higher compaction at the bottom than at the middle and top of the grain bed. This might be as a result of the use of a slim rectangular test box as the grain container.

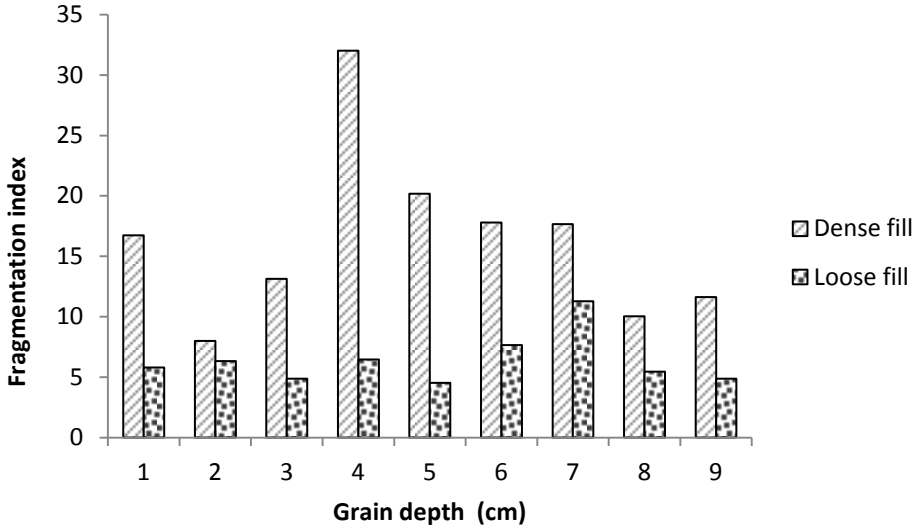

Figure 4.5: Fragmentation index distribution for loose and dense fill along the bed depth.

The ferret major axis ratio (FMR) was used to describe the geometric shape of pores inside loose and dense fill grain bulk (Igathinathane, 2008). It is defined as the ratio of the ferret diameter to the major axis diameter (equation 4.2). Ferret diameter is the diameter of a circle having the same area as the object (pores).

$$FMR = \frac{D_f}{a} \tag{4.2}$$

where:
$FMR =$ ferret major axis ratio
$D_f =$ ferret diameter(pixel)
$a =$ major axis diameter (pixel)

The FMR is equal to one when pore's shape is circular. It was found that FMR for the dense fill was 0.78 ±0.1, and 0.54 ±0.1. FMR did not vary much along the grain bed for both the fill methods (fig.4.6). The variation was 1.2% from the bottom to the top of the bin for the dense fill, and 14.3% from the bottom to the top of the bin for the loose fill.

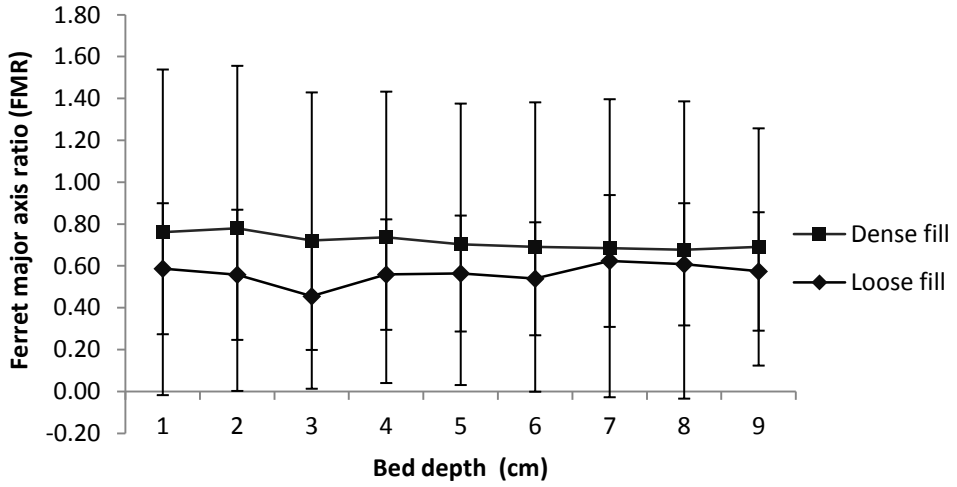

Figure 4.6: Pore shape distribution for loose and dense fill along the bed depth. (Error bar = Standard deviation)

4.3. Effect of flow rate on tortuosity

The average length of airflow path increased as the flow rate increased, and this consequently led to increase in tortuosity. Specifically, as the flow rate increased from 0.25 to 0.60 L s^{-1}, the average tortuosity increased from 1.17 to 1.31 for the loose fill, and from 1.20 to 1.38 for the dense fill (table 4.2).

Table 4.2: Average tortuosity and flow velocity at different flow rates and fill density.

Flow rate (L sec^{-1})		0.25	0.45	0.6
Loose Fill	Tortuosity	1.17 ±0.04†	1.22 ±0.10	1.31 ±0.05
	Velocity(cm s^{-1})	17.28 ±3.00	23.77 ±5.00	27.13 ±2.00
Dense Fill	Tortuosity	1.19 ±0.02	1.30 ±0.07	1.38 ±0.01
	Velocity (cm s^{-1})	12.49 ±4.70	16.87 ±1.10	19.65 ±5.00

† Standard deviation.

The effect of flow rate on tortuosity was found to be statistically significant $\alpha = 0.05$ (table 4.3). Increase in tortuosity with increased flow rate was probably due to increased "branching" or "spreading" of the flow within the grain bulk. As the flow rate increased, more flow branches (channels) developed, and these branches would have greater flow path lengths or higher tortuosity.

Table 4.3: ANOVA results for the effect of flow rate and fill density on tortuosity

Source	df	SS	MS	F	Significance
Fill density	1	0.01742	0.01742	5.19	0.0418
Flow rate	2	0.07854	0.03927	11.70	0.0015
Interaction	2	0.00201	0.00101	0.30	0.7465
Error	12	0.04027	0.00336		
Total	17	0.13824			

Tracked-thresholded images showed that the total flow path area was 203.73 cm^2 for 0.6 L s^{-1} and 122.34 cm^2 for 0.25 L s^{-1}. This indicated that the flow path covered by smoke for the higher flow rate (0.6 L s^{-1}) was about 50% greater than that when the flow rate was lower (0.25 L s^{-1}) (fig. 4.7). In other words, more flow channels existed, and the flow was more tortuous at higher airflow rate

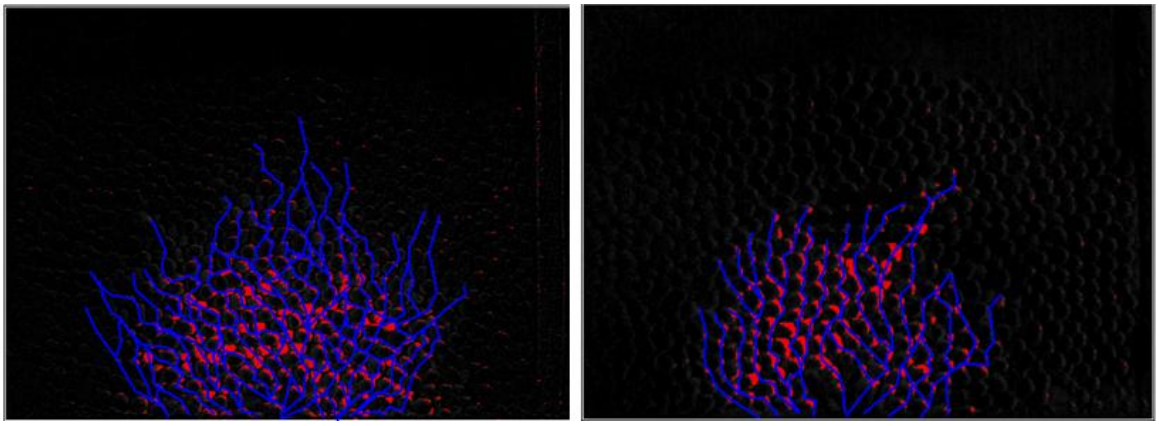

(a) (b)

Figure 4.7: Tracked-threshold images for loose fill at flow rates of (a) 0.60L s^{-1} and (b) 0.25L s^{-1}

This same trend was observed by Yu et al. (2006) in their study for the determination of tortuosity in porous compact made uni-axial compression sodium chloride; they concluded that the tortuosity values increased as the propagation speed increased. Tortuosity has been considered by many researchers as a geometrical property (Hilmi and Chilingarian, 2000; Garrouch et al., 2001; Barrande et al., 2007 Lihua and Chen, 2007; Arthur et al., 2011).

However, results from this study showed that tortuosity was not only a geometrical property that depends on the pore space geometry, but also depends on the characteristics of the flowing fluid inside the porous medium. It is possible to have different values of tortuosity for different flow processes in the same porous medium. Koponen et al. (1996) stated that the preferred definition of tortuosity should be based on the flow context and the porous structure of the medium. In this study, the results showed that tortuosity increased with increased flow rate (fig. 4.8). This observation agreed with the statement made by Francisco et al. (2011) and Manuel et al. (1999): tortuosity is a function of the flow velocity because the flow path length turns out to be a function of the fluid flow, as well as the system microstructure. Different values of tortuosity would be obtained in the same system depending on the flow rates (Francisco et al., 2011). This means that tortuosity is not exclusively a property of the porous medium microstructure.

Airflow resistance in grain bulks is related to its tortuosity (Gayathri et al., 2007). The increase in tortuosity value observed in this study, as the flow rate increases further validates the conclusions from several researchers that increase in airflow rate increases the resistance of airflow in grain bulk because the “tortuousness” of the flow increases as the flow rate increases(Rajabipour et al., 2001;Jekayinfa, 2006; Kenghe et al., 2012).

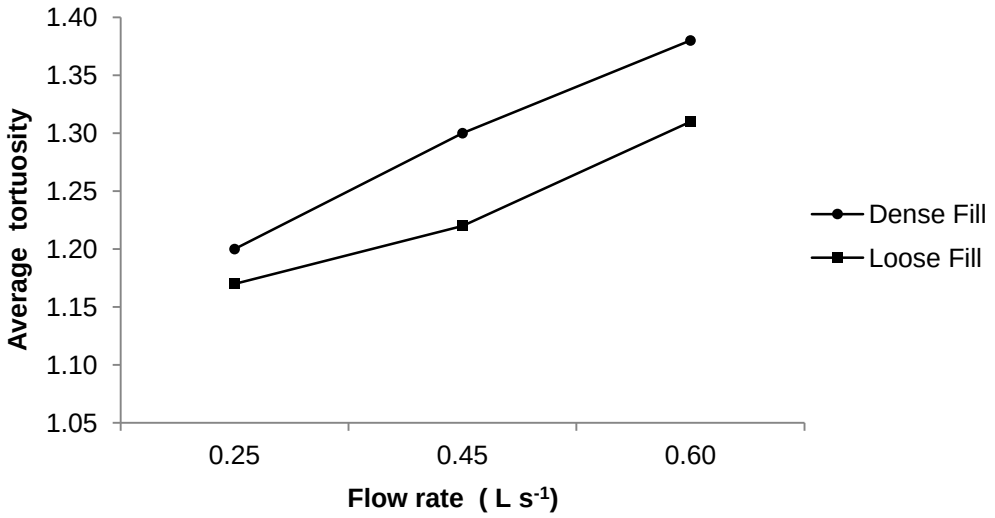

Figure 4.8: Effect of flow rate and fill density on the average tortuosity**.**

4.4. Effect of fill density on tortuosity

The density had a significant effect (α = 0.05) on tortuosity (table 4.3). The results indicated that tortuosity increased as the density changed from loose fill to dense fill. For 0.25, 0.45 and 0.60 L s^{-1} flow rates, the average tortuosity value changed from 1.17 to 1.20, 1.22 to 1.30 and 1.31 to 1.38 from loose to dense fill, respectively. This increase in tortuosity with increasing bulk density was attributed to the reduction in pore space. The higher number of disconnected flow paths inside the dense fill grain may likely be the cause of the increase in tortuosity value, because the smoke (air) had to find alternative paths when disconnected path was encountered.

A greater degree of waviness in flow path was caused by the application of higher pressure to the grain bulk (greater degree of compaction) (Hilmi et al., 2010). The total number of tracked smoke paths was 16 for the loose fill at 0.25 L s^{-1}, while the total number of the tracked smoke path was 24 for the dense fill at 0.25 L s^{-1} (fig.4.9). This signifies that more, but smaller channels existed in the dense fill compared to the loose fill at the same flow rate.

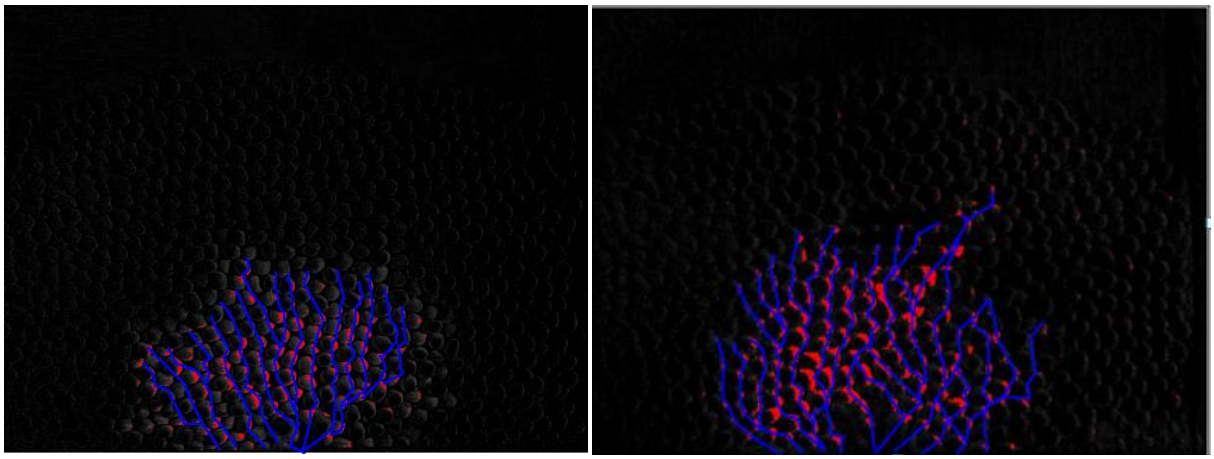

(a) (b)

Figure 4.9: Tracked - threshold image at 0.25L s^{-1} for (a) loose fill and (b) dense fill.

Tortuosity was significantly (α=0.05) affected by the porosity of the grain bulk. Similar, observations have been made by other researchers that tortuosity increases as the porosity reduces due to increase in the bulk density of the porous medium (Koponen et al., 1996; Manuel et al., 1999; Garrouch et al., 2001; Barrande et al., 2007 Lihua and Chen, 2007; Cedric, 2009; Rahul et al.,2010; Arthur et al., 2011).

Cedric et al. (2009) used two different methods for measuring the tortuosity of sandstone and clay soil from X-ray and electron topographic reconstructions, and concluded that tortuosity increased with reduction in the porosity of the porous media. Manuel et al. (1999) used imaging techniques to investigate 2D models of binary and mixed porous media constructed with spherical particles and concluded that tortuosity was affected by the volume fraction in the simulated porous media. Rahul et al. (2010) stated that air flow through fibrous porous media increasingly became less tortuous (lower tortuosity) with increasing porosity.

4.5. Effect of flow rate on flow velocity

The ANOVA statistical test results indicated that airflow rate had a significant (α = 0.05) effect on the flow velocity (table 4.4).

Table 4.4: ANOVA results for fill density and flow rate on average flow velocity

Source	df	SS	MS	F	Pr >F
Fill density	1	183.5528	183.5528	14.94	0.0020
Flow rate	2	222.2425	111.1212	9.05	0.0040
Interaction	4	5.9971	2.9985	0.24	0.7872
Error	12	147.4181	12.2848		
Total	17	559.2104			

The flow velocity increased as the air flow rate increased as expected. The results showed that as the flow rate increased from 0.25 to 0.60 L s^{-1}, the average flow velocity increased from 17.3 to 27.1 cm s^{-1} for the loose fill, and from 12.49 to 19.65 cm s^{-1} for the dense fill (fig. 4.10). Using the formula for Reynolds number for packed bed (equation 4.3), the flow in the grain bulk was classified as a mixed flow (laminar and turbulent flow) because the Reynolds was calculated to be 1553.4 for the loose fill and 921.9 for the dense fill which are both between 10 and 2000.

$$Re = \frac{\rho v D}{\mu(1-\varepsilon)} \tag{4.3}$$

where:

Re = Reynolds' number (Laminar flow condition apply when $Re < 10$ and turbulent flow condition when $Re > 2000$) (Sinnott, 2005)

v = mean superficial velocity (flow velocity) (m s^{-1})

ε = Porosity (decimal)

D = Spherical diameter (m)

μ = viscosity of air (kg m^{-1} s^{-1})

ρ = density of air (kg m^{-3})

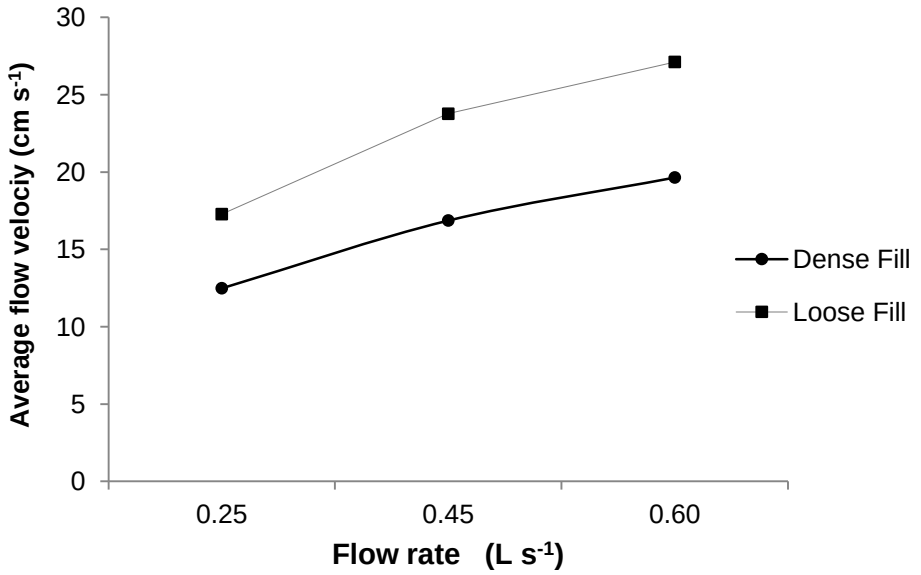

Figure 4.10: Effect of flow rate and fill density on average flow velocity.

4.6. Effect of fill density on flow velocity

The ANOVA statistical analysis results in table 4.4 shows that the fill density had a significant (α = 0.05) effect on the flow velocity. The flow velocity decreased as the fill density changed from loose to dense fill (fig. 4.10). For 0.25, 0.45 and 0.60 L s^{-1} flow rates, the average flow velocity changed from 17.3 to 12.5 cm s^{-1}, 23.77 to 16.9 cm s^{-1} and 27.1 to 19.7 cm s^{-1} from loose to dense fill, respectively.

The reduction in the flow velocity maybe as a result of reduction in the size of the pores as the fill density changed from loose to dense fill, which caused more “branching” of the airflow path. Smoke (air) flowed through the larger pores between the grain kernels more easily and lost less energy in the loose fill than in dense fill. The fan performance might have also contributed to the reduction in the flow velocity of the smoke (air) inside the grain bulks, since the flow rate output of the fan might decrease because of increase in the resistance to air flow in the dense fill.

It has been observed that flow velocity inside grain bulk was not uniform because of variation in pore size in the grain bulk (Neethirajan et al., 2008). For any particular flow path, the flow velocity changed randomly from one point to another along the path because the geometry of a typical flow path was extremely complex, with continuous changes in sectional area, shape and orientation along the flow path. Hence, flow velocity along a path could vary by several orders of magnitude (Maciej et al., 2008; Arthur et al., 2011). In general, the flow velocity decreased from the bottom to the top, as expected (fig. 4.11). For a given airflow rate of 0.25 L s^{-1} the flow velocity was about 70 to 20 cm s^{-1} from the bottom to top region of the bin. (fig. 4.11a).

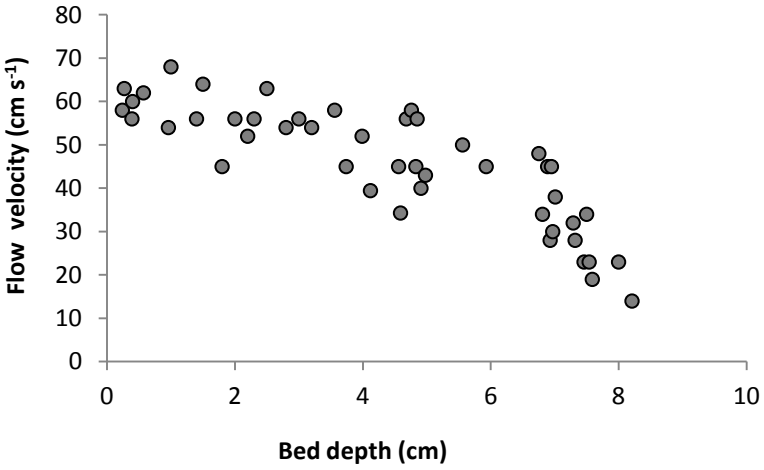

(a)

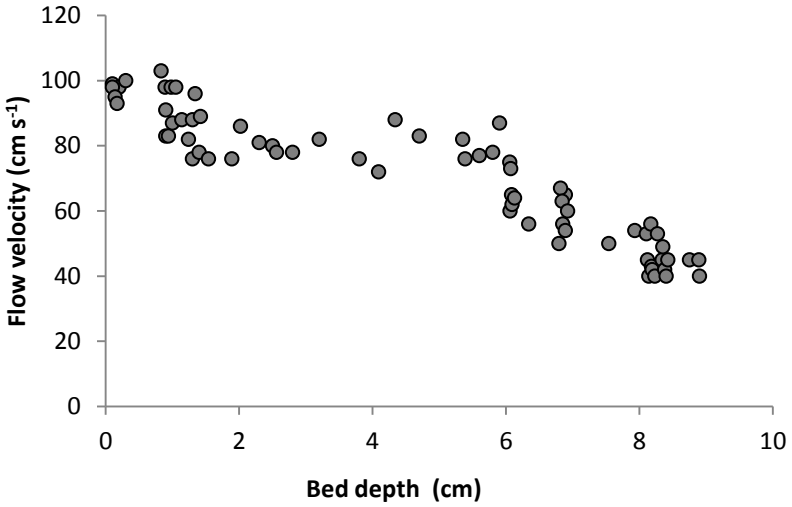

(b)

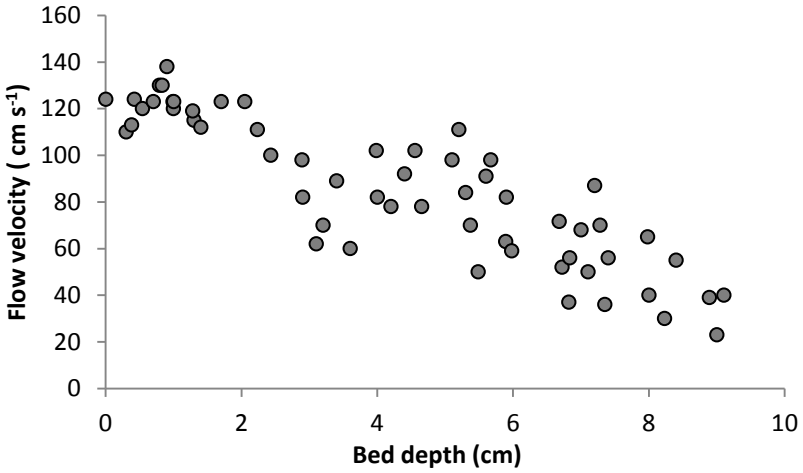

(c)

Figure 4.11: Flow velocity distribution of a random selected path at (a) 0.25 L s^{-1}, (b) 0.45 L s^{-1} and (c) 0.60 L s^{-1}

4.7. Multiple flow paths in grain bulk

When air flows from point A to B in a grain bulk, multiple paths are possible. In this study, the flow paths in the grain bulk were characterized into longest, shortest and fastest paths and their respective tortuosity and velocities were calculated.

The influence of the flow rate and the fill density on the tortuosity and velocity of the shortest, longest and fastest path follow similar trends as the average total flow paths discussed earlier. That is, the tortuosity of the shortest, longest, and fastest path increased with increase in flow rate. However, the effect on the fastest path was more pronounced (figs.4.12, 4.13, and 4.14).

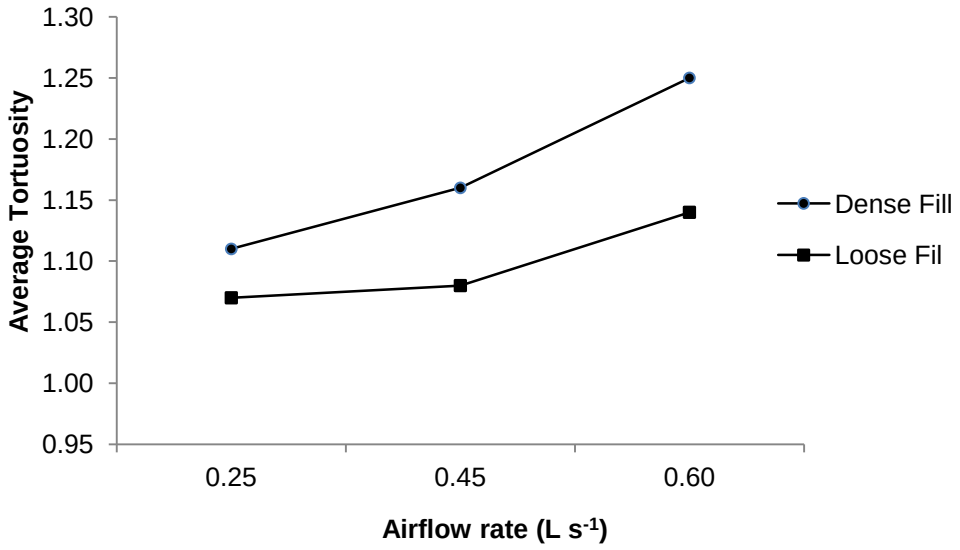

Figure 4.12: Effect of flow rate and fill density on tortuosity of the shortest path.

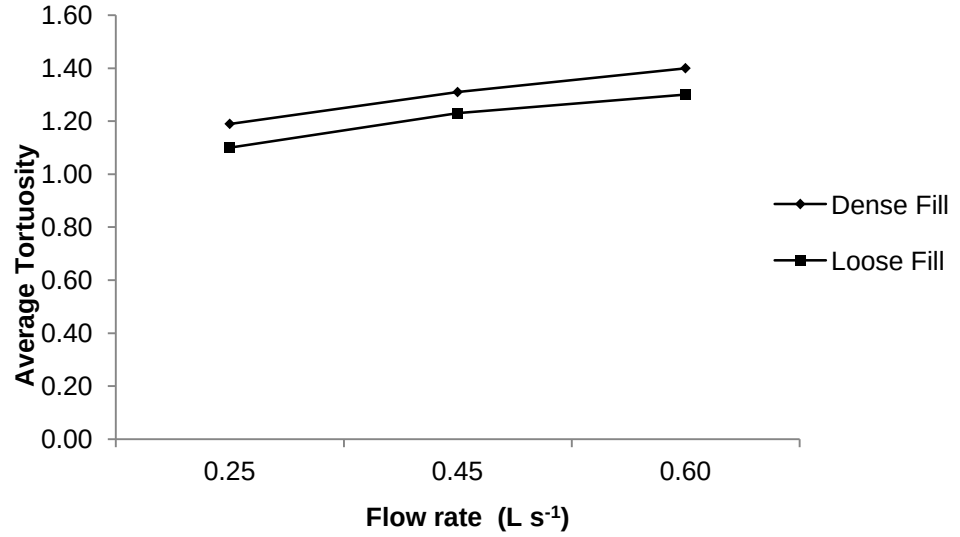

Figure 4.13: Effect of flow rate and fill density on tortuosity of fastest path.

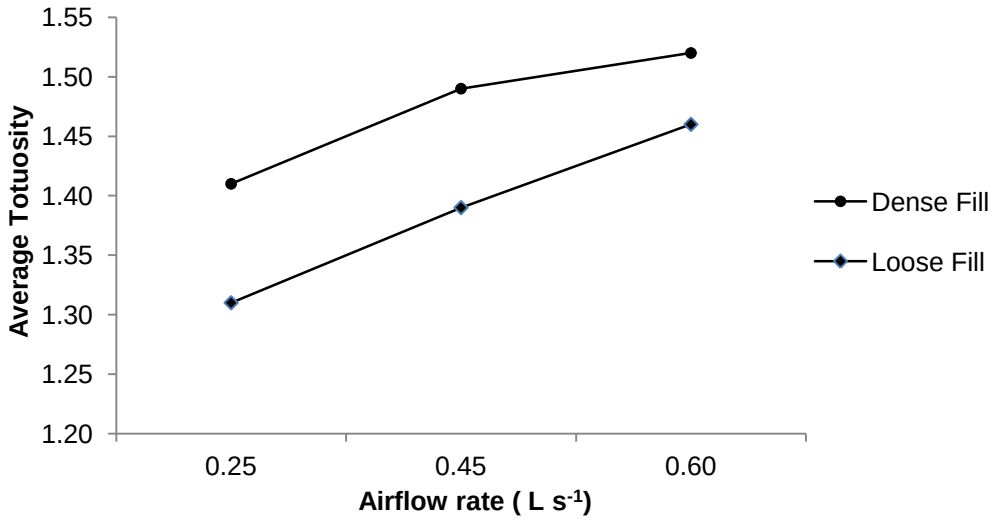

Figure 4.14: Effect of flow rate and fill density on tortuosity of longest path.

As the flow rate increased from 0.25 to 0.60 L s^{-1}, the average tortuosity of the shortest path increased by about 14% for the loose fill, 15% for the dense fill. For the longest path, as the flow rate increased from 0.25 to 0.60 L s^{-1}, the average tortuosity of the longest path increased by about 18% for the loose fill, and 13 % for the dense fill. For the fastest path, as the flow rate increased from 0.25 to 0.60 L s^{-1}, the average tortuosity increased from 24 % for the loose fill, and 28% for the dense fill.

It was of great interest to observe that the tortuosity of the fastest paths, though not the same as the tortuosity of the shortest paths, was always very close to the tortuosity of the shortest path at a lower flow rate. However, at high flow rate, the tortuosity of the fastest path was very close to that of the longest path observed. This observation is in consistent with the observation made by Yu et al. (2006) in their study of measuring flow path length as a measure of tortuosity in porous compact. They observed that when the propagation speed was low the fastest path stayed rather straight and short and the tortuosity was only marginally higher than one. At low flow speed (flow rate) the “branching” of the smoke flow through the grain bulk reduced drastically, unlike at high flow rate. The tortuosity of the shortest path is always smaller than the tortuosity of the fastest path. This connote that the shortest path is not the fastest

possible path inside the grain bulk. Although, the fastest path was longer than the shortest path for both the loose and dense fill, its thickness might be wider compare to the thickness of the shortest path. Hence, more smoke (air) flow through it since flow will follow the path of least resistance.

Also, Yu et al. (2006) concluded that the tortuosity values increased as the propagation speed increased for the porous compact, which is consistent with the results obtained in this study. It should be noted that the tortuosity values obtained in this study for the entire flow paths fell within the tortuosity range of 1.0 to 1.6, which was estimated by Yu et al. (2006). And also the average shortest path tortuosity from this study, was 1.14, which approximately equal to the values of tortuosity for the shortest path obtained theoretically by Wojciech et al. (2012) and experimental values obtained with CT image by Neethirajan et al. (2006) (1.15 and 1.14 respectively). Comparing the results of average tortuosity from this study with the results predicted from two empirical and theoretical equations shows that the measured tortuosity values in this study are within the range of those calculated by various theoretical and empirical equations (Table 4.5)

Table 4.5: Comparison of experimental and predictions results

	Loose Fill ($\varphi = 0.39$)	Dense Fill ($\varphi = 0.27$)	References
Experiment	1.23	1.30	
Theoretical $\tau^2 = 2 - \varphi$	1.27	1.35	Petersen (1958)
Theoretical $\tau^2 = 1 - \ln\varphi/2$	1.21	1.28	Akanni et al. (1987)
Empirical, P=0.41 $\tau^2 = 1 + P\ln\varphi/2$	1.38	1.54	Comiti and Renaud (1989)
Empirical; C=2 $\tau^2 = 1 - C\ln\varphi$	1.69	1.89	Boudreau (1996)

Table 4.6: Average tortuosity and velocity of the flow paths for the shortest, longest, fastest path at different flow rates and fill density.

Flow rate (L/sec)		0.25			0.45			0.6	
		Shortest Path	Longest Path	Fastest Path	Shortest Path	Longest Path	Fastest Path	Shortest Path	Longest Path	Fastest Path
Loose Fill	Tortuosity	1.02 ±0.045†	1.31 ±0.07	1.11 ±0.03	1.09 ±0.04	1.39 ±0.11	1.23 ±0.05	1.16 ±0.01	1.49 ±0.13	1.35 ±0.05
	Velocity (cm/sec)	12.51 ±1.78	17.00 ±2.60	22.73 ±3.00	29.22 ±10.00	24.03 ±5.00	39.65 ±2.00	21.54 ±2.40	11.04 ±1.94	42.69 ±0.05
Dense Fill	Tortuosity	1.11 ±0.05	1.41 ±0.17	1.19 ±0.01	1.15 ±0.02	1.49 ±0.17	1.31 ±0.01	1.26 ±0.04	1.54 ±0.07	1.39 ±0.04
	Velocity (cm/sec)	9.85 ±3.90	11.96 ±11	12.50 ±4.77	11.84 ±8.30	9.89 ±10	33.89 ±23	17.15 ±4.32	18.48 ±11	39.35 ±19

†SD

For the three characterized airflow paths (shortest, longest, and fastest paths), the flow velocity was found to be randomly distributed as the airflow rate increased and as fill density changed from loose to dense fill, no definite trends were observed (figs. 4. 15 and 4.16), except that the velocity increased with the flow rate for the fastest paths for both loose and dense fill.

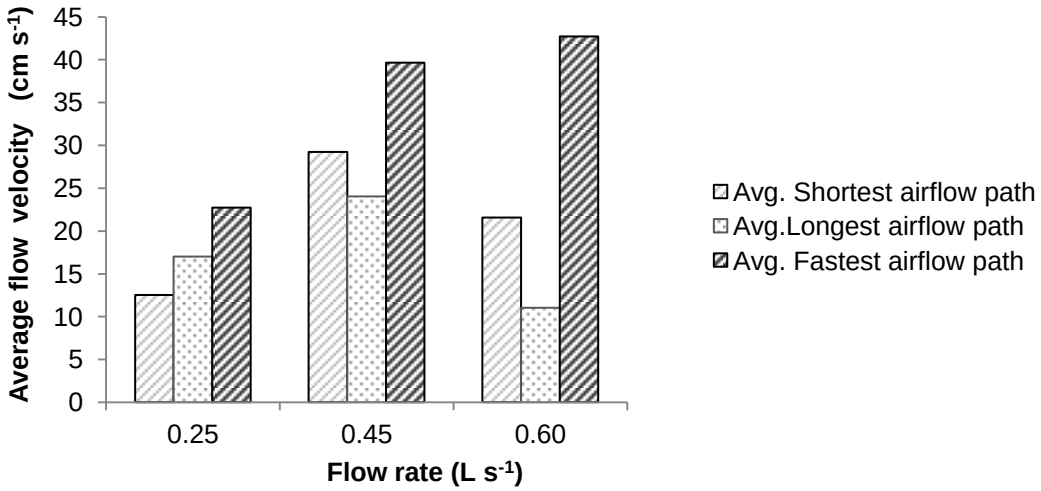

Figure 4.15: Effect of flow rate on flow velocity of the shortest, longest and fastest path for loose fill.

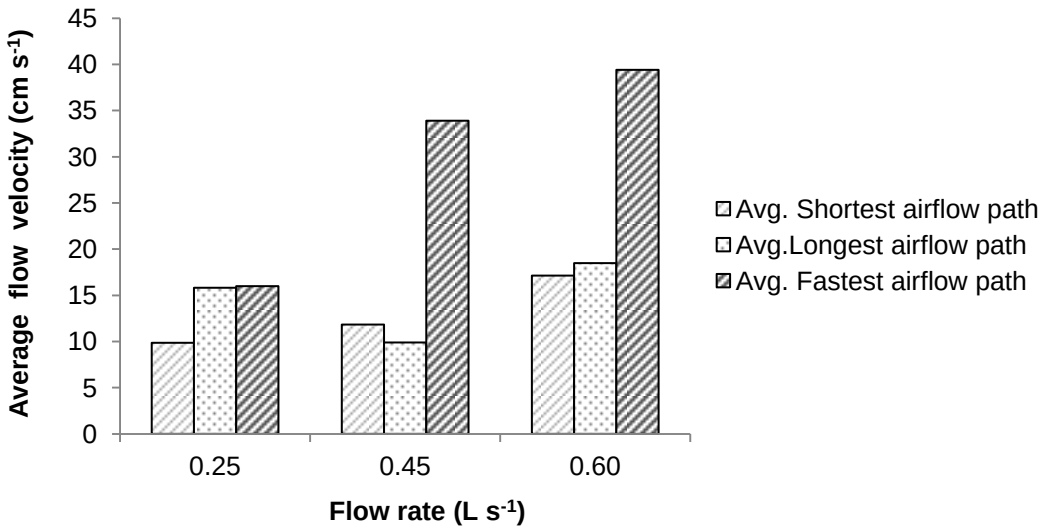

Figure 4.16: Effect of flow rate on flow velocity of the shortest, longest and fastest path for dense fill.

However, the random distribution of flow velocity observed for the shortest, longest, and the fastest path, further shows that air flow in grain bulk is not uniform (Kaponen et al, 1996; Maciej et al., 2008; Duda et al., 2011; Maciej and Koza, 2012). The non-uniformity of the resistance to airflow inside grain bulk explained the reason for random distribution of flow velocity, for the shortest, longest and the fastest path in the grain bulk.

5. CONCLUSIONS AND RECOMMENDATIONS

5.1. Conclusions

1. This study demonstrated that the direct measurement of tortuosity by smoke flow visualization was effective.
2. Tortuosity increased with airflow rate. As the flow rate increased from 0.25 to 0.60 L s^{-1} the average tortuosity increased from 1.17 to 1.31 for the loose fill, and from 1.20 to 1.38 for the dense fill. This meant that tortuosity was not only a geometrical property that depends on the pore space geometry, but also was dependent on the characteristics of flow through the porous medium. It is possible to have different values of tortuosity for the same porous medium under different flow conditions.
3. Tortuosity increased as the bulk density increased. For 0.25, 0.45 and 0.60 L s^{-1} flow rates, the average tortuosity value changed from 1.17 to 1.20, 1.22 to 1.30 and 1.31 to 1.38 respectively, when the density increased from 652 Kg m^{-3} (loose fill) to 755 Kg m^{-3} (dense fill).
4. The tortuosity for the fastest path was always greater than that of the shortest. In other words, the shortest path was not the fastest path. However, the tortuosity of the fastest path was close to the shortest path at low airflow rate (L s^{-1}), and at high airflow (0.60 L s^{-1}) rate the tortuosity of the fastest path was close to that of the longest path. At low flow rate the "branching" of the smoke flow through the grain bulk reduced drastically, unlike at high flow rates.
5. The pore channels (air path) were more connected in the loose fill than in the dense fill, with fragmentation index of about 21% higher than that of the dense fill. The pore space of the loose fill was 51.2% lower than the dense fill. And, while the shape in the dense fill is close to a circle with an average FMR value 0.78 $\pm$0.1, loose fill have an average FMR value of 0.54 $\pm$0.1.

5.2. Significance of the study

This study presented a method for direct measurement of tortuosity in grain bulks using smoke visualization and imaging processing techniques. And this method may lead to a new avenue for determination of air flow resistance in grain bulks. The traditional method of determining airflow resistance was based on empirical relations that do not apply to conditions other than those under which the experiments were conducted. Smoke visualization coupled with imaging processing techniques provides a powerful tool for researchers to investigate airflow through grain bulks at a microscopic level, and this may lead to the development of new mechanistic models for predicting airflow resistance through grain bulks.

Tortuosity has been considered by many researchers as a geometry property, which is a constant for a porous material. However, results from this study showed that tortuosity was not only a geometry property varying with the pore space geometry, but also depended on the characteristics of the flowing fluid inside the porous medium. This sheds new light on the understanding of tortuosity.

5.3. Recommendations

1. Other common grain, with different shape such as wheat should be used for the test, in order to study if shape or size of the grain has any effect on the tortuosity and the flow velocity. Effect of other factors such as moisture content maybe studied.
2. The design of the test bin should be changed slightly to be able to carry out the visualization test on the grain bulk with smoke flowing through the grain bulk from the horizontal direction, to evaluate the directional sensitivity or anisotropic pore structure behaviour on tortuosity.

3. Test should be conducted for measuring the tortuosity and the flow velocity though grain bulk using full perforation at the bottom of the test bin. Most of the aeration systems uses in the farm employ full perforation of the bottom for introduction of air into the grain bulk.
4. Image J plug-in(s) which can be used specifically for analyzing tortuosity, flow velocity, or any other important parameters (such as residence time, flow thickness etc) of flow in grain bulk can be developed in order to improve the process of analyzing air flow visualization images of grain bulk.

References

Adams, J. M.1972. Storage loss assessment techniques: A biologist view. Tropical Products Institute, paper presented at GASGA Serminar. Feb 6-7, 1973, TPI London.

Adrian, R. J.1991. Particle imaging techniques for experiment fluid mechanics*. Ann. Rev. Fluid Mech.* 23:261-304.

Akanni, K. A., J. W. Evans, I. S. Abramson. 1987. Effective transport coefficient in heterogeneous media. *Chemical Engineering Science* 42: 1945-1954.

Akpinar, E. K., and Y. Bicer. 2004. Modeling of the drying of eggplants in thin-layers. *International Journal of Food Sci.* and Technol. 39:1-9.

Alagusundaram, K., and D. S. Jayas. 1990. Airflow resistance of grains and oilseeds. *Postharvest News and Information* 1(4):279 -283.

Arthur, D., K. Zbigniew, and M. Mota. 2011. Hydraullic tortuosity in arbitrary porous media flow. *Physical Review E.* 84 (3):132-140.

Arthur, F., Y. Yang,and L. T.Wilson.2011.Utilization of a web-based model for aeration management in stored rough rice. *J. Econ. Entomol* 104:702-708.

ASABE Standard.2011. ASAE R2011. D272.3: Resistance to airflow of grains, seeds, other agricultural products and perforated metal sheet. St Joseph Mich.: ASABE.

ASABE Standard.1996. ASAE R2011. D272.3: Resistance to airflow of grains, seeds, other agricultural products and perforated metal sheet. St Joseph Mich.: ASABE.

ASABE Standard.1998. ASAE R2008.S352.2: Moisture measurement – Grain and seeds. St Joseph Mich.: ASABE.

Ashvin, K. G., Z. F. Anthony, R. Kanishkn, J. D. Andrew, J. L. Robert and S. H. Micheal. 2011. *Magnetic Resonance in Medicine* 67(4):1013-1021.

Astarita, T., G. Cardone, G. M. Carlomagno. 2006. Infrared thermography: an optical method in heat transfer and fluid flow visualization. *Optics and Laser in Engineering* 44:261- 281.

ASTM Standard. 2005. ASTM F1877-05: Standard practice for characterization of particles. West Conshohocken, Pa.: ASTM International.

ASTM Standard. 2007. ASTM C29-07: Standard test method for bulk density (“unit weight”) and voids in aggregate. West Conshohocken, Pa.: ASTM International.

Attia, M. 2005. Effects of petro physical rock properties on tortuosity factor. *J. Pet. Sci. Eng* 48: 1851-98.

Bakker-Arkema, F. W., R. J. Patterson, and W. G. Bickert.1969. Static pressure-airflow relationship in packed beds of granular biological materials such as cherry. *Transaction of the ASAE* 12(1):134-136.

Barrande, M., R. Bouchet, and R. Denoyel. 2007. Tortuosity of porous particles. *Ann. Chem.* 79: 9115 -9121.

Bear, J. 1972. Dynamic of fluids in porous media. 1st.ed. New York: Dover Publisher.

Bernard, P. B. and J. R. M. Filip.2006. Predicted tortuosity of muds. *Geology* 34 (8):693-696.

Boudreau, M. P.1996. The diffusive tortuosity of fine-grained unlithified sediments. *Geochimica et Cosmochimica Acta* 60:3139-3142.

Brakel, J. V., and P.M. Heertjes. 1974. Analysis of diffusion in macro porous media in terms of porosity, tortuosity and constrictivity factor. *Intl. J. Heat. Transfer* 17: 1093 -1099.

Brooker, D. B., F. W. Bakker-Arkema, and C. W. Hall.1974. Drying cereal grains. 2ed. Westport, Conn. USA: The AVI publishing Company.

Buchgraber, M., A. Al-Dossary, C. M. Ross, and A. R. Kovscek. 2012. Creation of a dual – porosity micro model for pore level visualization of multiphase flow. *Journal of petroleum Scince and Engineering* 86:27-28.

Calderwood, D. L. 1973. Resistance to airflow of rough brown and milled rice. *Trans. of the ASAE* 16: 525-532.

Carman, P. C. 1937. Fluid flow through a granular bed. Trans. Inst. Chem. Eng. 15:150 -156.

Cedric, G. J., A. J. Bons, S. Blacher, J. H. Dunsmuir, and A. H. Tsou. 2009. Practical method for measuring the tortuosity of porous materials from binary or grey-tone tomographic reconstructions*. AICHE J*.55 (8): 2000-2012.

Cenkowski, S., and Q. Zhang. 1995. Engineering properties of grains and oil seeds. In: Stored grain ecosystems, 411-463. US.: New York Dekker.

Chang, C. S. 1988. Measuring density and porosity of grain kernels using a gas pycnometer. Cereal Chem. 65(1): 13-15

Choudhary, G., and C. Horvath. 1997. Dynamic of capillary electro chromatography experimental study on the electrosomtic flow and conductance in open and packed capillaries. J. Chromatogr. 781: 161-183.

Clementson, C. L., K. E. Ileleji, and K. A. Rosentrater. 2010. Evaluation of measurement procedures used to determine the bulk density of distillers dried grains with soluble (DDGS). *Transaction of the ASAE* 53(2)485-490.

Comiti, J., and M. Renaud. 1989. A new model for determining mean structure parameters of fixed beds from pressure drop measurement: application to beds packed of parallelepipedal particles*. Chem. Eng*. Sci. 44: 1539-1545.

Cornell, D., and D. L. Katz. 1953. Flow of gasses through consolidated media. *Ind. Eng. Chem.* 45:2145 -2152.

Crozza, D. E., A. M. Pagano, and M. S. Nolasco. 1995. Resistance to airflow of bulk oat seeds. *J. Latin. American Applied Research* 25: 249-252.

Crozza, D. E. and A. M. Pagano. 2006. Modeling resistance to airflow through beds of agrpyron and corn estimation of power ventilation. *Latin American Applied Research 36*:7-14.

Dogu, G., and J. M. Smith. 1975. A dynamic method for catalyst diffusivities. AIChE. J. 21: 58-64.

Dullian, F. A. 1991. Porous Media: Fluid transport and pore structure. 2nd. ed. Waltham, MA: Academic Press.

Dutta, S. K., V. K. Nema, and R. K. Bhardwaj. 1988. Physical properties of gram. *J. Agric. Engng. Res.* 39: 259 -268.

Dykhuizen, R. C. and W. H.Casey.1989. An analysis of solute diffusion in rocks. *Geochimica et Cosmochimica Acta* 53:2797-2805.

Ergun, S. 1952. Fluid flow through packed columns. *Chem. Engr. Progr*. 48(2): 89-94.

Falk, E., M. Stefano, P. Dimitris, and P. Thomas. 2012. Digital holography from shadow graphic phase estimates. Optical Letters 37(4):504 -511.

Fang, C., and G. M. Campbell. 2008. Effect of measurement method and moisture content on wheat kernel density measurement. *Trans. IChemE.* 78:179-186.

Faris, S. R., L. S. Gournay, L. B. Lipson, and T.S. Webb. 1954. Verification of tortuosity equations. *Bull. Am. Assoc. Pet*. Geol. 38: 2226-2234.

Fashina , O. F. 2007. Physical properties of peanut hull pellets. ASABE paper No. 076161. St. Joseph, Mich.: ASAE.

Fellah, Z. E. A., W. Fellah. W. Lauriks and C. Depollier. 2003. Direct and inverse scattering of transient acoustic waves by a slab of rigid porous material. *J. Acoust. Soc. Am.* 113: 61 - 73.

Flinn, P. W., D. W. Hagstrum, and C. R. Muir.1997. Effects of time of aeration, bin size, and latitude of insect populations in stored wheat: a simulation study. *J. Econ. Entomol.* 90:646-651.

Florence, C., B. Marjorie, S. Laurent, and M. Jacques. 2008. Porous media and water vapour sorption of heap-based materials. *Contruction and Building Materials* 22:1271-1280.

Flurry. 2003. Dye as a tracer for vadose zone hydrology. *Reviews of Geophysics* 41(1):1002.

Foster, T. P., and E. L. Parrott. 1990. Release of highly water – soluble medicinal compounds from inert, heterogeneous matrices in physical mixtures. *J. Pharm. Sci.* 79: 806-810.

Francisco, J. V., and M. L. Peter.2011. The role of tortuosity in upscaling. *Trans. Porous. Med.* 88:1-30.

Friesen, O. H., and D. N. Huminicki.1986. Evaluation of grain airflow resistance characteristics and air delivery systems. *Canadian Agricultural Engineering* 28:107-115.

Garrouch, A. A, and H. M. S. Lababidi. 1995. An Inverted petrophysical model for shay sands. *In sittu* 19: 125-232.

Gayathri, P., and D. S Jayas. 2007. Mathematical modeling of airflow distribution in grain bulks. ASABE paper No. 076226. St. Joseph, Mich.: ASAE.

Giner, S. A. and E. Denisienia.1996. Pressure drop through wheat as affected by air velocity moisture content and. *J. Agr. Eng. Res.* 63:73 – 86.

Giovanni, M. C. and L. de Luca. 1998. Infrared thermography for flow visualization and heat transfer measurement. www.ineer.org/events/ICEE/998/icee/papers176.pdf. Accessed on 14th July, 2012.

Gommes, C. J., A. J. Bons, S. Blacher, J. H. Dunsmuir, and A. H. Tsou. 2009. Practical method for measuring the tortuosity of porous materials from binary or grey-tone tomographic reconstructions. *AICHE J*. 55(8):2000-2012.

Hilmi, S. S., and V. C.George. 2000. Physical and mathematical aspect of tortuosity in regards to fluid flow and electric current conduction in porous media: example of Hibernia and Terra Nova reservoirs, offshore the eastern coast of *Canada. Energy source* 22:137-145.

Hood, T. J. A., G. R. Thorpes. 1992. The effects of the anisotropic resistance to airflow on the design of aeration systems for bulk stored grains. *Agricultural Engineering Australia* 21:18 -23.

Hukill, W. V., and N. C. Ives.1955. Radial airflow resistance of grain. *J. Agric. Eng.* 36(5):332-335.

Hunter, A. J. 1983. Pressure difference across an aerated seed bulk for some common duct and store cross section. *J. Agric. Eng.* Res. 28:437-450.

Ibrahim, D. 2007. The kinetics of forced convective air-drying of pumpkin slices. *Journal of Food Engineering* 27:243-248.

IGC, 2012. Grain Market Report: International Grains Council, London. Available at: www.igc.int/en/downloads/gmrsummary/gmrsummary.pdf. Accessed 14 Sept. 2012.

James, R. S., S. T. Micheal, L. I. Mathew, and G. L. Peter. 2005. Optical flow visualization systems for the cryogenic environment. *Rev. Sci.* 76:84.

Jasmine, E. 2000. Flow visualization for a micro air vehicle. Msc. Thesis. Toronto: University of Toronto, Department of Aerospace Science and Engineering.

Jayas, D. S., and N. D. G. White. 2003. Storage and drying of grain in Canada: low cost approaches. *Food control* 14:255-261.

Jekayinfa, S. O. 2006. Effect of airflow rate, moisture content and pressure drop on the airflow resistance of locust bean seed. *Agric. Eng. Intl.* 9:345-359.

Jian, C., D. Y. Yong, Y. J. Yuan, and D. L. Xiang. 2006. Pore network model and simulation transport process for grain. *Chemical Engineering and Technology* 34(7):1049 – 1056.

Kammath, J., B. Xu, S. H. Lee, and Y. C. Yortsos. 1998. Use of pore network models to interpret laborartory experiment on vugular rocks. Journal of petrol Science and Engineering 20:109-115.

Karababa, E. 2006. Physical properties of popcorn kernel. Journal of Food Engineering 72:100 - 107.

Kenghe, R. N., P. M. Nimkar, S. S. Shirkole, and K. J. Shinde. 2012. Airflow resistance in soybean. *Int. Agrophys* 26:137 -143.

Koponen, A., M.Kataja, and J.Timonen.1996. Tortuous flow in porous media. *Physical Review E*. 54(1):406-410.

Kozeny, J. 1927. Uber Kapillare leitung des wassers im boden. Sitzungbererichte der Akadamie der Wissenschaftung in Wein Abeilung 136: 271-301.

Kumar, A., W. E. Muir. 1986. Airflow resistance of wheat and barley affected by airflow direction, filling method and dockage. *Transaction of the ASAE* 29(6):1423-1426.

Lamond, W. J. and E. A.Smith.1982. Modeling low temperature drying of grain in anisotropic beds. In Proc. Third international drying symposium. Birmingham, England.

Leweke, T. 2012. Dye visualization - a method for investigation biomedical. *Current Pharmaceutical Biotechnology* 13(11): 2141-2152.

Lihua, S., and C.Zhangxin.2007. Critical review of the impact of tortuosity on diffusion. *Chemical Engineering Science* 62:3748 – 3755.

Lita, T., M. Murakami, T. Shimazaki, and H. Nagai. *Cryogenics* 36:943-956.

Lukaszuk, J., M.Molenda, J.Horabik,B.Szot, and M.D.Montross. 2008. Airflow resistance of wheat bedding as influenced by the filling method. J. Agric. Eng. Res. 54(2):50- 57.

Maciej, M., K. Arzhang, K. Zbigniew. 2008. Tortousity-porosity relation in the porous media flow. *Phys.Rev. E.* 78(2):1-8.

Maciej, M., and K. Zbigniew. 2012. How to calculate tortuosity easily. Wroclaw, Poland.: Institute of theoretical Physics.

MacMASTER, M. M.1962. Important aspect of kernel structure. *Transaction of the ASAE 5(2):247-249.*

Madamba, P. S., R. H. Driscoll, and K. A. Buckle.1994. Bulk density, porosity and resistance to airflow of garlic slices. *Drying Technology* 12(4):937-954.

Manuel, M., A. T. Jose, and Y. Alexander.1999. Image analysis of packed beds of spherical particles of different sizes. 15:59-68.

McGregor, T. J., D. J. Spence, and D. W. Coutts. 2008. Laser-based volumetric flow visualization by digital imaging off a spectrally coded volume. *Rev. Sci. Instrum*. 79(1):013710 –

Medeni, M. 2001. Drying, shrinkage and rehydration characteristics of kiwifruits during hot air and microwave drying. *Journal of Food Engineering* 48:177-182.

Metzger, J. E., P. D. Terry, and W. E. Muir. 1981. Performance of several axial –flow fans for grains bin ventilation. *Canadian Agricultural Engineering* 23(1):11-16.

Mohsenin, N. N. 1986. Physical properties of plant and animal materials: Structure, physical characteristics, and mechanical properties. New York, NY: Gordon and Breach Publisher

Mota, M., A. T. Jose, and Y. Alexander.1999. Image analysis of packed beds of spherical particles of different sizes. 15:59- 68.

Montross, M. D. and D. E. Maier. 2001. A new moisture equilibration theory to predict moisture movement in a non- aerated grain mass. ASABE paper No.016110. St. Joseph, Mich.: ASAE.

Montross, M. D., D. E. Maier, and K. Haghighi. 1982 Validation of a finite-element stored grain ecosystem model. *Transaction of the ASAE* 45(5):1465-1474.

Muller, T. J. 1983. Flow visualization by direct injection. In Fluid Mechanics Mesasurement, R.J. Goldstein.ed. 307-375. Washington.: Hemisphere.

Muir, W. E., S. Cenkowski, and Q.Zhang.2005. Physical characteristics of grain bulks. In: Grain Preservation Biosystems.

Narong, U., S. Somchart, P. Somkiat, and N. Adisak. 2006. A comparative study of pork drying using superheated steam and hot air. *Drying Technology* 24:1665-1672.

Navarro, S., and R. Noyes. 2002. The mechanics and physics of modern grain aeration management. Boca Raton: CRC Press.

Navarro, S., R. T. Noyes, M. Casada, and F.H. Arthur. 2012. Chapter 11: Aeration of grain. In Stored Product Protection, 121 – 134. D.W.Hagstrum, T.W.Phillips, and G. Cuperus, ed. Kansas, US.: Kansas State University.

Neethirajan, S., C. Karunakaran., D.S.Jayas, and N.D.G. White. 2006. X- ray computed tomography image analysis to explain the airflow resistance differences in grain bulks. *Biosystems Engineering* 94: 545 - 555.

Neilsen, J. 1998. Pressure from flowing granular solids in silos. *Phil. Trans. Roy. Soc. Lon* 356: 2667

Nimkar, P. M., and P. K. Chattopahyay. 2002. Airflow resistance of green gram. *Biosystems Engineering* 82(4): 407-414.

Nimmo,J. R. 2004. Porosity and pore size distribution. In: Encyclopedia of Soils in Environment: London Eslsevier

Nunata, D., M. W. Hayee, A. Bunyajitradulya, and S.Eiamsa. 2012. Visualiztion of flow and heat transfer characteristics for swirling impinging jet. *International Communication in Heat and Mass Transfer* 39:640 – 648.

Ohyama, R., K.Inoue, and J.S.Chang. 2007. Schlieren optical visualization for transient EHD induced flow in a stratified dieelectric liquid under gas-phase ac corona discharge. Journal Phys. D. Appl. Phys. 40:573-578.

Pagano, A. M., S. M. Crozza, and S. M. Nolasco. 2000. Airflow resistance of oat seeds: effect of the airflow direction, moisture content, and foreign material. *J. Drying Tech.* 18: 457 - 468.

Papsdokostaki, K. G., S. G. Amarantos and J. H. Petropoulos. 1998. Kinetic of release of particulate solutes incorporated in cellusic polymer matrices as a function of the solute solubility and polymer sealability. Sparingly soluble solutes. *J. Appl. Polym. Sci.* 67:227 - 287.

Peter. F.1993. Flow visualization in fluid mechanics*. Rev. Sci*. Instrum 64:1-9.

Petersen, E. E.. 1958. Diffusion in a pore of varying cross section. *American Institute of Chemical Engineering Journal* 4:343-345.

Peterson, J. W., J.D.Mathew, and L. K.Kimberly. 2000. A laborartory simulation of toluene clean up by air sarging of water-saturated sands. *Journal of Hazardous Material* 72:167-178.

Pirson, S. J. 1983. Geological Well Log Analysis. Houston, TX: Gulf Publishing.

Rahul, V., B. L. Pamela, and S. Abdel-Fattah. 2010. New approach for determining tortuosity in fibrous porous media. *Journal of Engineered Fibers and Fabrics* 5(3):7-15

Rajabipour, A., F. Shahbazi, S. Mohtasebi, and A. Tabatabaefar. 2001. Airflow resistance in walnut. J. Agric. Sci. Tech. 3: 257-264.

Richard, O. P., and L. Z Gary.1988. Monitoring Natural air corn drying – a demonstration project. *Applied Engineering Agriculture* 4(1) :84 -87.

Rigby, S. P. and L. F.Gladden.1996. NMR and Fractal modeling studies of transport in porous media. *Chemical Engineering Science* 51(10):2263- 2272.

Robert, J. G. and E.H. Glenn. 1972. Density and porosity changes of shelled corn during drying. Transaction of the ASAE 15(3):523 -525.

San, W. and Y.Ge. 1982. Two methods for low density flow visualization. In Flow visualization, Merzkirch, ed. 421-425. Washington, DC.:Hemisphere.

Savicki, K. 2004. Resistance of bulk poppy seeds to airflow. Biosys. Eng. 89(4): 435-443.

Schumacher, B. and G. A. Von. 1953. Init elecktronenstrahlen. *Ann. Physik.* 6:404 -411

Shahbazi, F. 2011. Resistance of bulk chickpea seeds to airflow. *J. Agric. Sci. Tech.* 13:996-676.

Shedd, C. K. 1951. Some new data on resistance of grains to airflow. *J. Agric. Eng.* 32: 493-495.

Shinohara, K., K. Shoji, and T. Tanaka. 1972. Mechanism of size segregation of particles in filling a hopper. *Ind. Eng. Chem. Proc. Des. Dev.* 11(3):369 -376.

Sidney, D. 2000. Review mercury porosimetry: An appropriate method for the measurement of pore size distribution in cement-based material. *Cement and Concreate Research* 30:1517-1525.

Sinnott, R. K. 2005. Chemical Engineering Design. 4th.ed. Oxford, UK: Butterworth-Heinemann.

Standish, N.1985. Studies of size segregation in filling and emptying a hopper. *Powder Tech.* 45(1): 43-56.

Stephen, L. E., and G. H. Foster. 1976. Grain bulk properties as affected by mechanical grain spreader. *Transaction of the ASAE 19* (3): 345-358.

Stuart, O. N. 1980. Moisture-dependent kernel and bulk density relationship for wheat and corn. *Transaction of the ASAE* 23(1):139-143.

Stuart, O., Nelson, D.S.C, and S.Trabelsi. 2011. Sensing grain and seed moisture from dielectric properties*. Int. J. Agric and Biol.* Eng 4(1):75-81.

Suman, R. and D.Ruth. 1993. Formation factor and tortuosity of homogeneous porous media.*Transport in porous media* 12:185-206.

Tang, Z. and C. Cenkowski. 2000. Dehydration dynamics of potatoes in superheated steam and hot air. Canadian Agricultural Engineering 42(1):6.1-6.13.

Tamari, S. 2004. Optimum design of the constant gas pycnometer for determining the volume of solid particles. Meas. Sci. Technol 15:549-558.

Tomadakis, M.M. and S.V. Sotischos. Ordinary and transition regime diffusion in random fiber strucrures. American Institute of Chemical Engineers Journal 39(3):397 – 412.

Ueta, Y.,K.Yanaka., M.Murakami, H.Nagai, and H.Yanget.2002. Cryogenics 42:645 –

Van Brakel, J. and P.M.Heerrtjes.1974. Analysis of diffusion in macroporous media in terms of a porosity, a tortuosity and a constrictivity factor. International Journal of Heat and Mass Transfer 17:1093-1103.

Vertucci, C. W. and E. E. Ross. 1990. Theoretical basis of protocols for seed storage. Plant Physiol. 94(3):1019-1023.

Wang, R., T. Pavlin, M.S. Rosen, R. W. Mair, D.G. Cory, and R. L.Walsworth. 2005. Xenon NMR measurement of permeability and tortuosity in rsservoir rocks. *Magnetic Resonance Imaging* 23: 329-331.

Webb, P. A. 2001. An introduction to the physical characterization of materials by mercury intrusion porosimetry with emphasis on reduction and presentation of experiment data. http://www.particletesting.com/docs/intro_mip.pdf (Assessed, June 28, 2012).

Winsauer, W. O., H. M. Shearin, P. H. Masson, and M. Williams. 1952. Resistivity of brine saturated sands in relation to pore geometry. Bull. Am. Assoc. Petrol. Geol. 36: 253.

Wojciech, S., Q. Zhang, and L. Chuanyum. 2012. Predicting tortuosity for airflow through porous beds consisting of randomly packed spherical particles. Transp. Porous. Med. 93: 431-451.

Wolfram, V. F., W. H.Timo, T.Holger , and S.Hans-Peters. 2008. Smoke surfaces: an interactive flow visualization techniques inspired by real worlds flow experiments. IEEE Transaction on visualization and Computer graphics 14(6):1396 – 1403.

Woodcraft, A., P.Lucas, R.Matley, W.Wong, and J.Low. 1999. Temp. Phys. 114:109

Wu, J., and Y. Boming. 2007. A fractal resistance model for frlow through porous media. *Intl. J. of Heat and Mass Transfer* 50:3925-3932.

Wyllie, M. R. J., and M. B. Spangler. 1966. Application of Electrical resistivity measurement to problem of fluid flow in porous media. *AIChE. J* 12: 321-329

Yu, S.., O.G.Clark, and J.J. Leonard. 2005. Airflow measurement in passively aerated compost. *Canadian Biosystems Engineering* 47(6): 39 -45.

Yu, S.W., J. Lucas., V. Van., W. Henderik, and V. Kess. 2006. The determination of relative path length as a measure for tortuosity in compacts using image analysis. *Euro. J. of Pharm. Sci*. 28: 434-440.

Yuichi, H., and T. Oguchi. 2005. Evaluation of gravel sphericity and roundness based on surface area measurement with a lasser scanner. *Computer and Geoscience* 31:735-741.